Review

# Prospects for charged Higgs searches at the LHC

A. G. Akeroyd[1], M. Aoki[2], A. Arhrib[3,4], L. Basso[5], I. F. Ginzburg[6], R. Guedes[7], J. Hernandez-Sanchez[8,9],
K. Huitu[10], T. Hurth[11], M. Kadastik[12], S. Kanemura[13], K. Kannike[12], W. Khater[14], M. Krawczyk[15,a],
F. Mahmoudi[16,17], S. Moretti[1], S. Najjari[15], P. Osland[18,b], G. M. Pruna[19], M. Purmohammadi[18],
A. Racioppi[12], M. Raidal[12], R. Santos[20,21], P. Sharma[22], D. Sokołowska[15], O. Stål[23], K. Yagyu[1], E. Yildirim[1]

[1] School of Physics and Astronomy, University of Southampton, Highfield, Southampton SO17 1BJ, UK
[2] Institute for Theoretical Physics, Kanazawa University, Kanazawa 920-1192, Japan
[3] Département de Mathématique, Faculté des Sciences et Techniques, Université Abdelmalek Essaâdi, B. 416, Tangier, Morocco
[4] LPHEA, Faculté des Sciences-Semlalia, B.P. 2390 Marrakesh, Morocco
[5] CPPM, Aix-Marseille Université, CNRS-IN2P3, UMR 7346, 163 Avenue de Luminy, 13288 Marseille Cedex 9, France
[6] Sobolev Institute of Mathematics SB RAS, Novosibirsk University, 630090 Novosibirsk, Russia
[7] IHC, Instituto de História Contemporanea, FCSH - New University of Lisbon, Lisbon, Portugal
[8] Facultad de Ciencias de la Electrónica, Benemérita Universidad Autónoma de Puebla, Apdo. Postal 542, C.P. 72570 Puebla, Puebla, Mexico
[9] Dual C-P Institute of High Energy Physics, Colima, Mexico
[10] Department of Physics, and Helsinki Institute of Physics, University of Helsinki, Gustaf Hällströmin katu 2, P.O.Box 64, 00014 Helsinki, Finland
[11] PRISMA Cluster of Excellence and Institute for Physics (THEP), Johannes Gutenberg University, 55099 Mainz, Germany
[12] National Institute of Chemical Physics and Biophysics, Rävala 10, 10143 Tallinn, Estonia
[13] Department of Physics, University of Toyama, 3190 Gofuku, Toyama 930-8555, Japan
[14] Department of Physics, Birzeit University, PO Box 14, Birzeit, West Bank, Palestine
[15] Faculty of Physics, University of Warsaw, Pasteura 5, 02-093 Warsaw, Poland
[16] Univ Lyon, Univ Lyon 1, ENS de Lyon, CNRS, Centre de Recherche Astrophysique de Lyon, UMR5574, 69230 Saint-Genis-Laval, France
[17] Theoretical Physics Department, CERN, 1211 Geneva 23, Switzerland
[18] Department of Physics and Technology, University of Bergen, Postboks 7803, 5020 Bergen, Norway
[19] Paul Scherrer Institute, 5232 Villigen, PSI, Switzerland
[20] Centro de Física Teórica e Computacional, Faculdade de Ciências, Universidade de Lisboa, Campo Grande, Edifício C8, 1749-016 Lisbon, Portugal
[21] Instituto Superior de Engenharia de Lisboa - ISEL, 1959-007 Lisbon, Portugal
[22] Center of Excellence in Particle Physics (CoEPP), The University of Adelaide, Adelaide, SA, Australia
[23] Department of Physics, The Oskar Klein Centre, Stockholm University, 106 91 Stockholm, Sweden

**Abstract** The goal of this report is to summarize the current situation and discuss possible search strategies for charged scalars, in non-supersymmetric extensions of the Standard Model at the LHC. Such scalars appear in Multi-Higgs-Doublet models, in particular in the popular Two-Higgs-Doublet model, allowing for charged and additional neutral Higgs bosons. These models have the attractive property that electroweak precision observables are automatically in agreement with the Standard Model at the tree level. For the most popular version of this framework, Model II, a discovery of a charged Higgs boson remains challenging, since the parameter space is becoming very constrained, and the QCD background is very high. We also briefly comment on models with dark matter which constrain the corresponding charged scalars that occur in these models. The stakes of a possible discovery of an extended scalar sector are very high, and these searches should be pursued in all conceivable channels, at the LHC and at future colliders.

## 1 Introduction

In the summer of 2012 an SM-like Higgs particle ($h$) was found at the LHC [1,2]. As of today its properties agree with the SM predictions at the 20% level [3,4]. Its mass derived from the $\gamma\gamma$ and $ZZ$ channels is $125.09 \pm 0.24$ GeV [5]. However, the SM-like limit exists in various models with extra neutral Higgs scalars. A charged Higgs boson ($H^+$) would be the most striking signal of an extended Higgs sector, for example with more than one Higgs doublet. Such a discovery at the LHC is a distinct possibility, with or without

[a] e-mail: Maria.Krawczyk@fuw.edu.pl
[b] e-mail: Per.Osland@uib.no

supersymmetry. However, a charged Higgs particle might be rather hard to find, even if it is abundantly produced.

We here survey existing results on charged-scalar phenomenology, and discuss possible strategies for further searches at the LHC. Such scalars appear in Multi-Higgs-Doublet models (MHDM), in particular in the popular Two-Higgs-Doublet model (2HDM) [6,7], allowing for charged and more neutral Higgs bosons. We focus on these models, since they have the attractive property that electroweak precision observables are automatically in agreement with the Standard Model at the tree level, in particular, $\rho = 1$ [8–10].

The production rate and the decay pattern would depend on details of the theoretical model [6], especially the Yukawa interaction. It is useful to distinguish two cases, depending on whether the mass of the charged scalar ($M_{H^\pm}$) is below or above the top mass. Since an extended Higgs sector naturally leads to Flavor-Changing Neutral Currents (FCNC), these would have to be suppressed [11,12]. This is normally achieved by imposing discrete symmetries in modeling the Yukawa interactions. For example, in the 2HDM with Model II Yukawa interactions a $Z_2$ symmetry under the transformation $\Phi_1 \to \Phi_1, \Phi_2 \to -\Phi_2$ is assumed. In this case, the $B \to X_s \gamma$ data constrain the mass of $H^+$ to be above approximately 480 GeV [13]. A recent study concludes that this limit is even higher, in the range 570–800 GeV [14]. Our results can easily be re-interpreted for this new limit. Alternatively, if all fermion masses are generated by only one doublet ($\Phi_2$, Model I) there is no enhancement in the Yukawa coupling of $H^+$ with down-type quarks and the allowed mass range is less constrained. The same is true for the Model X (also called Model IV or lepton-specific 2HDM) [15,16], where the second doublet is responsible for the mass of all quarks, while the first doublet deals with leptons. Charged Higgs mass below $\mathcal{O}(M_Z)$ has been excluded at LEP [17]. Low and high values of $\tan\beta$ are excluded by various theoretical and experimental model-dependent constraints.

An extension of the scalar sector also offers an opportunity to introduce additional CP violation [18], which may facilitate baryogenesis [19].

Charged scalars may also appear in models explaining dark matter (DM). These are charged scalars not involved in the spontaneous symmetry breaking, and we will denote them as $S^+$. Such charged particles will typically be members of an "inert" or "dark" sector, the lightest neutral member of which is the DM particle ($S$). In these scenarios a $Z_2$ symmetry will make the scalar DM stable and forbid any charged-scalar Yukawa coupling. Consequently, the phenomenology of the $S^+$, the charged component of a $Z_2$-odd doublet, is rather different from the one in usual 2HDM models. In particular, $S^+$ may become long-lived and induce observable displaced vertices in its leptonic decays. This is a background-free experimental signature and would allow one to discover the $S^+$ at the LHC.

The SM-like scenario (also referred to as the "alignment limit") observed at the LHC corresponds to the case when the relative couplings of the 125 GeV Higgs particle to the electroweak gauge bosons $W/Z$ with respect to the ones in the SM are close to unity. We will assume that this applies to the lightest neutral, mainly CP-even Higgs particle, denoted $h$. Still there are two distinct options possible – with and without decoupling of other scalars in the model. In the case of decoupling, very high masses of other Higgs particles (both neutral and charged) arise from the soft $Z_2$ breaking term in the potential without any conflict with unitarity.

The focus of this paper will be the $Z_2$-softly broken 2HDM, but we will also briefly discuss models with more doublets. In such models, one pair of charged Higgs-like scalars ($H^+ H^-$) would occur for each additional doublet. We also briefly describe scalar dark matter models.

This work arose as a continuation of activities around the workshops "Prospects for Charged Higgs Discovery at Colliders", taking place every 2 years in Uppsala. The paper is organized as follows. In Sects. 2–4 we review the basic theoretical framework. In Sect. 5 we review charged Higgs decays, and in Sect. 6 we review charged-Higgs production at the LHC. Section 7 is devoted to an overview of different experimental constraints. Proposed search channels for the 2HDM are presented in Sect. 8, whereas in Sects. 9 and 10 we discuss models with several doublets, and models with dark matter, respectively. Section 11 contains a brief summary. Technical details are collected in appendices.

## 2 Potential and states

The general 2HDM potential allows for various vacua, including CP-violating, charge breaking and inert ones, leading to distinct phenomenologies. Here we consider the case when both doublets have non-zero vacuum expectation values. CP violation, explicit or spontaneous, is possible in this case.

### 2.1 The potential

We limit ourselves to studying the softly $Z_2$-violating 2HDM potential, which reads

$$
\begin{aligned}
V(\Phi_1, \Phi_2) = -\frac{1}{2} & \left\{ m_{11}^2 \Phi_1^\dagger \Phi_1 + m_{22}^2 \Phi_2^\dagger \Phi_2 + \left[ m_{12}^2 \Phi_1^\dagger \Phi_2 + \text{h.c.} \right] \right\} \\
& + \frac{\lambda_1}{2} \left( \Phi_1^\dagger \Phi_1 \right)^2 + \frac{\lambda_2}{2} \left( \Phi_2^\dagger \Phi_2 \right)^2 + \lambda_3 \left( \Phi_1^\dagger \Phi_1 \right) \left( \Phi_2^\dagger \Phi_2 \right) \\
& + \lambda_4 \left( \Phi_1^\dagger \Phi_2 \right) \left( \Phi_2^\dagger \Phi_1 \right) + \frac{1}{2} \left[ \lambda_5 \left( \Phi_1^\dagger \Phi_2 \right)^2 + \text{h.c.} \right].
\end{aligned}
$$

$$(2.1)$$

Apart from the term $m_{12}^2$, this potential exhibits a $Z_2$ symmetry,

$$(\Phi_1, \Phi_2) \leftrightarrow (\Phi_1, -\Phi_2) \quad \text{or} \quad (\Phi_1, \Phi_2) \leftrightarrow (-\Phi_1, \Phi_2). \tag{2.2}$$

The most general potential contains in addition two more quartic terms, with coefficients $\lambda_6$ and $\lambda_7$, and violates $Z_2$ symmetry in a hard way [6]. The parameters $\lambda_1$–$\lambda_4$, $m_{11}^2$ and $m_{22}^2$ are real. There are various bases in which this potential can be written, often they are defined by fixing properties of the vacuum state. The potential (2.1) can lead to CP violation, provided $m_{12}^2 \neq 0$.

## 2.2 Mass eigenstates

We use the following decomposition of the doublets (see Appendix A):

$$\Phi_1 = \begin{pmatrix} \varphi_1^+ \\ (v_1 + \eta_1 + i\chi_1)/\sqrt{2} \end{pmatrix}, \quad \Phi_2 = \begin{pmatrix} \varphi_2^+ \\ (v_2 + \eta_2 + i\chi_2)/\sqrt{2} \end{pmatrix}, \tag{2.3}$$

which corresponds to a basis where both have a non-zero, real and positive, vacuum expectation value (vev). Here $v_1 = \cos\beta \, v$, $v_2 = \sin\beta \, v$, $v = 2\, m_W/g$, with $\tan\beta = v_2/v_1$.

We adopt the mixing matrix $R$, between the scalar fields $\eta_1, \eta_2, \eta_3$ and mass eigenstates $H_1, H_2, H_3$ (for the CP-conserving case CP-even $h$, $H$ and CP-odd $A$, respectively) defined by

$$\begin{pmatrix} H_1 \\ H_2 \\ H_3 \end{pmatrix} = R \begin{pmatrix} \eta_1 \\ \eta_2 \\ \eta_3 \end{pmatrix}, \tag{2.4}$$

satisfying

$$R\mathcal{M}^2 R^{\mathrm{T}} = \mathcal{M}_{\mathrm{diag}}^2 = \mathrm{diag}\left(M_1^2, M_2^2, M_3^2\right), \quad M_1 \leq M_2 \leq M_3. \tag{2.5}$$

The rotation matrix $R$ is parametrized in terms of three rotation angles $\alpha_i$ as [20]

$$R = \begin{pmatrix} c_1\, c_2 & s_1\, c_2 & s_2 \\ -(c_1\, s_2\, s_3 + s_1\, c_3) & c_1\, c_3 - s_1\, s_2\, s_3 & c_2\, s_3 \\ -c_1\, s_2\, c_3 + s_1\, s_3 & -(c_1\, s_3 + s_1\, s_2\, c_3) & c_2\, c_3 \end{pmatrix} \tag{2.6}$$

with $c_i = \cos\alpha_i$, $s_i = \sin\alpha_i$, and $\alpha_{1,2,3} \in (-\pi/2, \pi/2]$. In Eq. (2.4), $\eta_3 \equiv -\sin\beta\,\chi_1 + \cos\beta\,\chi_2$ is the combination of $\chi_i$'s which is orthogonal to the neutral Nambu–Goldstone boson. In terms of these angles, the limits of CP conservation correspond to [21]

$H_1$ odd $(H_1 \equiv A)$ :   $\alpha_2 = \pm\pi/2,$

$H_2$ odd $(H_2 \equiv A)$ :   $\alpha_2 = 0, \alpha_3 = \pm\pi/2,$     (2.7)

$H_3$ odd $(H_3 \equiv A)$ :   $\alpha_2 = 0, \alpha_3 = 0.$

The charged Higgs bosons are the combination orthogonal to the charged Nambu–Goldstone bosons: $H^\pm = -\sin\beta\,\varphi_1^\pm + \cos\beta\,\varphi_2^\pm$, and their mass is given by

$$M_{H^\pm}^2 = \mu^2 - \frac{v^2}{2}(\lambda_4 + \mathrm{Re}\lambda_5), \tag{2.8}$$

where we define a mass parameter $\mu$ by

$$\mu^2 \equiv (v^2/2v_1 v_2)\mathrm{Re}\,m_{12}^2. \tag{2.9}$$

Note also the following relation arising from the extremum condition:

$$\mathrm{Im}\,m_{12}^2 = \mathrm{Im}\,\lambda_5 v_1 v_2. \tag{2.10}$$

## 2.3 Gauge couplings

With all momenta incoming, we have the $H^\mp W^\pm H_j$ gauge couplings [22]

$$H^\mp W^\pm H_j : \quad \frac{g}{2}[\pm i(\sin\beta\, R_{j1} - \cos\beta\, R_{j2}) + R_{j3}](p_\mu^j - p_\mu^\mp). \tag{2.11}$$

Specifically, for coupling to the lightest neutral Higgs boson, the $R$-matrix (2.6) gives

$$H^\mp W^\pm H_1 : \quad \frac{g}{2}[\pm i \cos\alpha_2 \sin(\beta - \alpha_1) + \sin\alpha_2](p_\mu - p_\mu^\mp). \tag{2.12}$$

The familiar CP-conserving limit is obtained by evaluating $R$ for $\alpha_2 = 0$, $\alpha_3 = 0$, $\alpha_1 = \alpha + \pi/2$, with the mapping $H_1 \to h$, $H_2 \to -H$ and $H_3 \to A$. In that limit, we recover the results of [6]:

$$H^\mp W^\pm h : \quad \frac{\mp ig}{2}\cos(\beta - \alpha)(p_\mu - p_\mu^\mp),$$

$$H^\mp W^\pm H : \quad \frac{\pm ig}{2}\sin(\beta - \alpha)(p_\mu - p_\mu^\mp), \tag{2.13}$$

$$H^\mp W^\pm A : \quad \frac{g}{2}(p_\mu - p_\mu^\mp).$$

The strict SM-like limit corresponds to $\sin(\beta - \alpha) = 1$, however, the experimental data from the LHC [3,4] allow for a departure from this limit[1] down to approximately 0.7, which we are going to allow in our study.

---

[1] Note that in the 2HDM, this factor cannot exceed 1.

In the following analysis, the gauge couplings to neutral Higgs bosons are also involved. They differ from the SM coupling by the factor ($V = W^\pm, Z$)

$$VVH_j : \quad \cos\beta R_{j1} + \sin\beta R_{j2}. \tag{2.14}$$

In particular, for $H_1$, this factor becomes $\cos(\beta - \alpha_1)\cos\alpha_2$. In the CP-conserving case, we have

$$
\begin{aligned}
VVh : &\quad \sin(\beta - \alpha), \\
VVH : &\quad \cos(\beta - \alpha), \\
VVA : &\quad 0.
\end{aligned} \tag{2.15}
$$

Note that the couplings (2.11) and (2.14) are given by unitary matrices, and hence satisfy sum rules. Furthermore, for any $j$, the relative couplings of (2.11) (the expression in the square brackets) and (2.14) satisfy the following relation [23]:

$$|(2.11)|^2 + [(2.14)]^2 = 1. \tag{2.16}$$

These relations are valid for both the CP-conserving and the CP-violating cases.

## 3 Theoretical constraints

The 2HDM is subject to various theoretical constraints. First, it has to have a stable vacuum,[2] what leads to so-called positivity constraints for the potential [24,29,30], $V(\Phi_1, \Phi_2) > 0$ as $|\Phi_1|, |\Phi_2| \to \infty$. Second, we should be sure to deal with a particular vacuum (a global minimum) as in some cases various minima can coexist [31–33].

Other types of constraints arise from requiring perturbativity of the calculations, tree-level unitarity [34–38] and perturbativity of the Yukawa couplings. In general, imposing tree-level unitarity has a significant effect at high values of $\tan\beta$ and $M_{H^\pm}$, by excluding such values. These constraints limit the absolute values of the $\lambda$ parameters as well as $\tan\beta$, the latter both at very low and very high values. This limit is particularly strong for a $Z_2$ symmetric model [33,39,40]. The dominant one-loop corrections to the perturbative unitarity constraints for the model with softly broken $Z_2$ symmetry are also available [41].

The electroweak precision data, parametrized in terms of $S$, $T$ and $U$ [42–48], also provide important constraints on these models.

**Table 1** The most popular models of the Yukawa interactions in the 2HDM (also referred to as "Types"). The symbols $u$, $d$, $\ell$ refer to up- and down-type quarks, and charged leptons of any generation. Here, $\Phi_1$ and $\Phi_2$ refer to the Higgs doublet coupled to the particular fermion. Also other conventions are being used in the literature; see Appendix B

| Model | $d$ | $u$ | $\ell$ |
|---|---|---|---|
| I | $\Phi_2$ | $\Phi_2$ | $\Phi_2$ |
| II | $\Phi_1$ | $\Phi_2$ | $\Phi_1$ |
| III | $\Phi_1$ $and$ $\Phi_2$ | $\Phi_1$ $and$ $\Phi_2$ | $\Phi_1$ $and$ $\Phi_2$ |
| X | $\Phi_2$ | $\Phi_2$ | $\Phi_1$ |
| Y | $\Phi_1$ | $\Phi_2$ | $\Phi_2$ |

## 4 Yukawa interaction

There are various models of Yukawa interactions; all of them, except Model III, lead to suppression of FCNCs at tree level, assuming some vanishing Yukawa matrices. The most popular is Model II, in which up-type quarks couple to one (our choice: $\Phi_2$) while down-type quarks and charged leptons couple to the other scalar doublet ($\Phi_1$). They are presented schematically in Table 1. For a self-contained description of the 2HDM Yukawa sector, see Appendix B.[3]

For Model II, and the third generation, the neutral-sector Yukawa couplings are

$$
\begin{aligned}
H_j b\bar{b} : &\quad \frac{-ig\,m_b}{2\,m_W}\frac{1}{\cos\beta}[R_{j1} - i\gamma_5\sin\beta R_{j3}], \\
H_j t\bar{t} : &\quad \frac{-ig\,m_t}{2\,m_W}\frac{1}{\sin\beta}[R_{j2} - i\gamma_5\cos\beta R_{j3}].
\end{aligned} \tag{4.1}
$$

Explicitly, for the charged Higgs bosons in Model II, we have for the coupling to the third generation of quarks [6]

$$
\begin{aligned}
H^+ b\bar{t} : &\quad \frac{ig}{2\sqrt{2}\,m_W} V_{tb}[m_b(1+\gamma_5)\tan\beta + m_t(1-\gamma_5)\cot\beta], \\
H^- t\bar{b} : &\quad \frac{ig}{2\sqrt{2}\,m_W} V_{tb}^*[m_b(1-\gamma_5)\tan\beta + m_t(1+\gamma_5)\cot\beta],
\end{aligned} \tag{4.2}
$$

where $V_{tb}$ is the appropriate element of the CKM matrix. For other Yukawa models the factors $\tan\beta$ and $\cos\beta$ will be substituted according to Table 6 in Appendix B.

As mentioned above, the range in $\alpha$ (or $\alpha_1$) is $\pi$, which can be taken as $[-\pi, 0]$, $[-\pi/2, \pi/2]$ or $[0, \pi]$. This is different from the MSSM, where only a range of $\pi/2$ is required [50], $-\pi/2 \le \alpha \le 0$. The spontaneous breaking of the symmetry and the convention of having a positive value for $v$ means that the sign (phase) of the field is relevant. This doubling of the range in the 2HDM as compared with the MSSM is the origin of "wrong-sign" Yukawa couplings.

---

[2] Here we perform an analysis at the tree level, for more advanced studies; see [24–28].

[3] The absence of tree-level FCNC interactions can also be obtained by imposing flavor space alignment of the Yukawa couplings of the two scalar doublets [49].

## 5 Charged Higgs-boson decays

This section presents an overview of the different $H^+$ decay modes, illustrated with branching ratio plots for parameter sets that are chosen to exhibit the most interesting features. Branching ratios required for modes considered in Sects. 8–10 are calculated independently.

As discussed in [6,51–55], a charged Higgs boson can decay to a fermion–antifermion pair,

$$H^+ \to c\bar{s}, \tag{5.1a}$$
$$H^+ \to c\bar{b}, \tag{5.1b}$$
$$H^+ \to \tau^+\nu_\tau, \tag{5.1c}$$
$$H^+ \to t\bar{b}, \tag{5.1d}$$

(note that (5.1b) refers to a mixed-generation final state), to gauge bosons,

$$H^+ \to W^+\gamma, \tag{5.2a}$$
$$H^+ \to W^+Z, \tag{5.2b}$$

or to a neutral Higgs boson and a gauge boson,

$$H^+ \to H_j W^+, \tag{5.3}$$

and their charge conjugates.

Below, we consider branching ratios mainly for the CP-conserving case. For the lightest neutral scalar we take the mass $M_h = 125$ GeV. Neither experimental nor theoretical constraints are here imposed (they have significant impacts, as will be discussed in subsequent sections). For the calculation of branching ratios, we use the software 2HDMC [55] and HDECAY [53,56]. As discussed in [56], branching ratios are calculated at leading order in the 2HDM parameters, but we include QCD corrections according to [57–59], and three-body modes via off-shell extensions of $H^+ \to t\bar{b}$, $H^+ \to hW^+$, $H^+ \to HW^+$ and $H^+ \to AW^+$. The treatment of three-body decays is according to Ref. [52].

For light charged Higgs bosons, $M_{H^\pm} < m_t$, Model II is excluded by the $B \to X_s\gamma$ constraint discussed in Sect. 7. For Model I (which in this region is *not* excluded by $B \to X_s\gamma$), the open channels have fermionic couplings proportional to $\cot\beta$. The gauge couplings (involving decays to a $W^+$ and a neutral Higgs) are proportional to $\sin(\beta - \alpha)$ or $\cos(\beta - \alpha)$, whereas the corresponding Yukawa couplings depend on the masses involved, together with $\tan\beta$.

The CP-violating case for the special channel $H^+ \to H_1 W^+$ is presented in Sect. 5.4.

### 5.1 Branching ratios vs. $\tan\beta$

Below, we consider branching ratios, assuming for simplicity $M_{H^\pm} = M_A$, in the low- and high-mass regions.

#### 5.1.1 Light $H^+$ ($M_{H^\pm} < m_t$)

For a light charged Higgs boson, such as might be produced in top decay, the $tb$ and $Wh$ channels would be closed, and the $\tau\nu$ and $cs$ channels would dominate. The relevant Yukawa couplings are given by $\tan\beta$ and the fermion masses involved. With scalar masses taken as follows:

$$M_{H^\pm} = M_A = 100 \text{ GeV}, \quad M_H = 150 \text{ GeV}, \tag{5.4}$$

we show in Fig. 1 branching ratios for the different Yukawa models.

Since the $\tau\nu$ and $cs$ couplings for Model I are the *same*, the branching ratios are independent of $\tan\beta$, as seen in the left panel. For Models X and II the couplings to $c$ and $\tau$ have different dependences on $\tan\beta$, and consequently the branching ratios will depend on $\tan\beta$. In the case of Model Y, the $cs$ channel is for $\tan\beta > \sqrt{m_c/m_s}$ controlled by the term $m_s \tan\beta$, which dominates over the $\tau\nu$ channel at high $\tan\beta$.

#### 5.1.2 Heavy $H^+$ ($M_{H^\pm} > m_t$)

Below, we consider separately the two cases where one more neutral scalar is light, besides $h$, this being either $H$ or $A$. For a case where the two channels $hW$ and $HW$ are open, whereas $AW$ is not, exemplified by the masses

$$M_{H^\pm} = M_A = 500 \text{ GeV}, \quad M_H = 130 \text{ GeV}, \tag{5.5}$$

we show in Fig. 2 branching ratios for the different Yukawa models. Two values of $\sin(\beta - \alpha)$ are considered, 1 and 0.7. For comparison with Sect. 5.2, we have drawn dashed lines at $\tan\beta = 1$, 3 and 30.

For Model I (left part of Fig. 2), the dominant decay rates are to the heaviest fermion–antifermion pair and to $W$ together with $h$ or $H$ (for the considered parameters, both $h$ and $H$ are kinematically available). Model X differs in having an enhanced coupling to tau leptons at high $\tan\beta$; see Table 6 in Appendix B. If the decay to $Wh$ is kinematically not accessible, the $\tau\nu$ mode may be accessible at high $\tan\beta$.

For Model II (right part of Fig. 2), the dominant decay rates are to the heaviest fermion–antifermion pair at low and high values of $\tan\beta$, with $hW$ or $HW$ dominating at medium $\tan\beta$ (if kinematically available). At high $\tan\beta$ it is the down-type quark that has the dominant coupling. Hence, modulo phase space effects, the $\tau\nu$ rate is only suppressed by the mass ratio $(m_\tau/m_b)^2$. Model Y differs from Model II in *not* having enhanced coupling to the tau at high values of $\tan\beta$.

**Fig. 1** Light charged-Higgs branching ratios vs. tan $\beta$. *Left* Models I and X, *right* Models II and Y. The *panel on the right* is only for illustration, such a light $H^+$ is excluded for the models II and Y
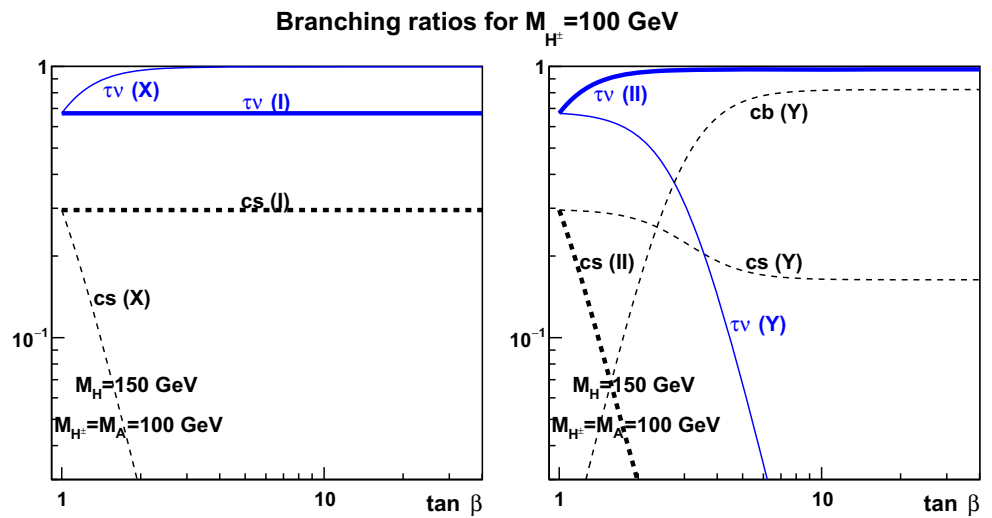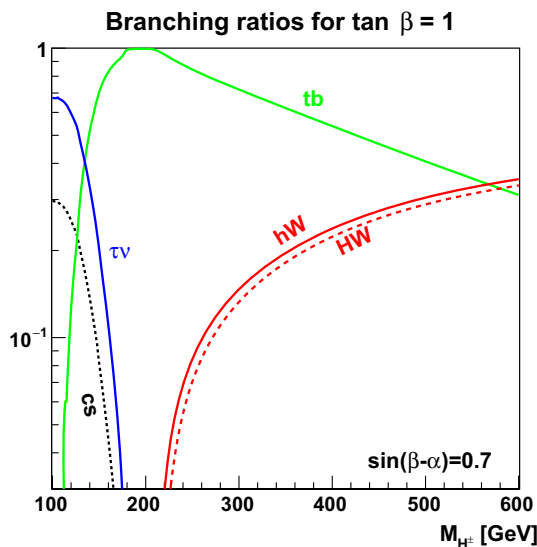


**Fig. 2** Heavy charged-Higgs branching ratios vs. tan $\beta$ for two light neutral Higgs bosons $h$ and $H$. *Left* Models I and X, *right* Models II and Y. *Upper two panels* $\sin(\beta - \alpha) = 1$, *lower panels* $\sin(\beta - \alpha) = 0.7$. The *dashed vertical lines* are for comparison with Figs. 3–4
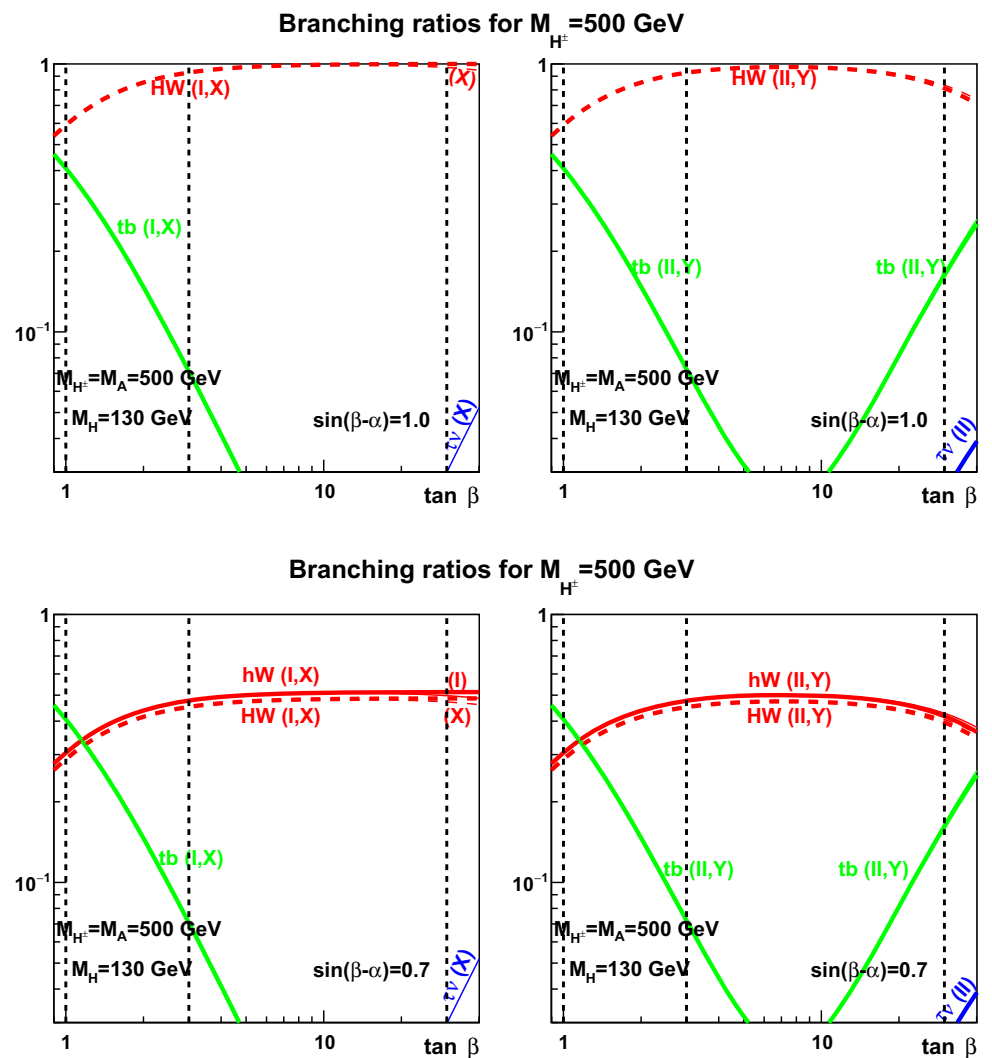


Whereas the couplings and hence the decay rates to $hW$ and $HW$, for fixed values of $\sin(\beta - \alpha)$, are independent of tan $\beta$, the branching ratios are not. They will depend on the strengths of the competing $tb$ Yukawa couplings. The strength of the $hW$ channel increases with $\cos^2(\beta - \alpha)$, and is therefore absent in the upper panels where $\sin(\beta - \alpha) = 1$.

## Branching ratios for tan β = 1



**Fig. 3** Charged-Higgs branching ratios vs. $M_{H^\pm}$, for $\tan\beta = 1$ and $\sin(\beta - \alpha) = 0.7$. Here, two light neutral Higgs bosons $h$ and $H$ (125 and 130 GeV) are considered

It should also be noted that if the $Wh$ channel is not kinematically available, the $tb$ channel would dominate for all values of $\tan\beta$. The $\tau\nu$ channel, which may offer less background for experimental searches, is only relevant at higher $\tan\beta$, and then only in Models II and X.

When $A$ is light, such that the channels $H^+ \to W^+ A$ and $H^+ \to W^+ h$ are both open, whereas $H^+ \to W^+ H$ is not, the situation is similar to the previous case, with the $HW$ mode replaced by the $AW$ mode. The choice $\sin(\beta - \alpha) = 1$ turns off the $H^+ \to W^+ h$ mode [see Eq. (2.13)], and there is a competition among the $WA$ and the $tb$ modes, except for the region of high $\tan\beta$, where also the $\tau\nu$ mode can be relevant.

### 5.2 Branching ratios vs. $M_{H^\pm}$

In Figs. 3 and 4 we show how the branching ratios change with the charged Higgs mass. Here, we have taken $\tan\beta = 1$ (Fig. 3), 3 and 30 (Fig. 4), together with the neutral-sector masses

$$(M_H, M_A) = (130\ \text{GeV}, M_{H^\pm}) \tag{5.6}$$

(note that here we take $M_{H^\pm} = M_A$), and we consider the two values $\sin(\beta - \alpha) = 1$ and 0.7, corresponding to different strengths of the gauge couplings (2.13).

The picture from Figs. 1 and 2 is confirmed: at low masses, the $\tau\nu$ channel dominates, whereas at higher masses, the $tb$ channel will compete against $hW$ and $HW$, if these channels are kinematically open and not suppressed by some particular values of the mixing angles.

Of course, for $\tan\beta = 1$ (Fig. 3), all four Yukawa models give the same result. Qualitatively, the result is simple. At low

masses, the $\tau\nu$ and $cs$ channels dominate, whereas above the $t$ threshold, the $tb$ channel dominates. There is, however, some competition with the $hW$ and $HW$ channels. Similar results hold for $\sin(\beta - \alpha) = 1$, the only difference being that the $HW$ branching ratio rises faster with mass, and the $hW$ mode disappears completely in this limit. Even below the $hW$ threshold, branching ratios for three-body decays via an off-shell $W$ can be significant [52]. The strength of the $hW$ channel is proportional to $\cos^2(\beta - \alpha)$, and it is therefore absent for $\sin(\beta - \alpha) = 1$ (not shown).

At higher values of $\tan\beta$ (Fig. 4), the interplay with the $HW$ and $hW$ channels becomes more complicated. At high charged-Higgs masses, the $HW$ rate can be important (if kinematically open). On the other hand, the $hW$ channel can dominate over $HW$, because of the larger phase space. Here, we present the case of $\sin(\beta - \alpha) = 0.7$. The case of $\sin(\beta - \alpha) = 1$ is similar, the main difference is a higher $HW$ branching ratio, while the $hW$ channel disappears. It should be noted that three-body channels that proceed via $hW$ and $HW$ can be important also below threshold, if the $tb$ channel is closed.

### 5.3 Top decay to $H^+ b$

A light charged Higgs boson may emerge in the decay of the top quark

$$t \to H^+ b, \tag{5.7}$$

followed by a model-dependent $H^+$ decay. In Model I possible channels are $H^+ \to \tau^+ \nu$ and $H^+ \to c\bar{s}$, as shown in Fig. 1. For the former case, the product BR$(t \to H^+ b) \times$ BR$(H^+ \to \tau^+ \nu)$ is shown in Fig. 5 for three values of $\tan\beta$. Note that recent LHC data have already excluded a substantial region of the low-$\tan\beta$ and low-$M_{H^\pm}$ parameter region in Model I; see Sect. 7.2.3.

### 5.4 The $H^+ \to H_1 W^+$ partial width

In this section we consider the decay mode $H^+ \to H_1 W^+$, allowing for the possibility that the lightest Higgs boson, $H_1$, is not an eigenstate of CP.

The $H^+ \to H_1 W^+$ coupling is given by Eq. (2.12). The partial width, relative to its maximum value, is given by the quantity

$$\cos^2 \alpha_2 \sin^2(\beta - \alpha_1) + \sin^2 \alpha_2, \tag{5.8}$$

which is shown in Fig. 6. We note that there is no dependence on the mixing angle $\alpha_3$. If $\alpha_3 = 0$ or $\pm\pi/2$, then CP is conserved along the axis $\alpha_2 = 0$ with $H_1 = h$.

In the alignment limit,

$$\alpha_1 = \beta, \quad \alpha_2 = 0, \tag{5.9}$$

**Fig. 4** Charged-Higgs branching ratios vs. $M_{H^\pm}$, for $\tan\beta = 3$ and 30, with two light neutral Higgs bosons $h$ and $H$ (125 and 130 GeV). *Left* Models I and X, *right* Models II and Y. *Top* $\sin(\beta - \alpha) = 0.7$, *bottom* $\sin(\beta - \alpha) = 1$

**Branching ratios for tan β = 3**



**Branching ratios for tan β = 30**
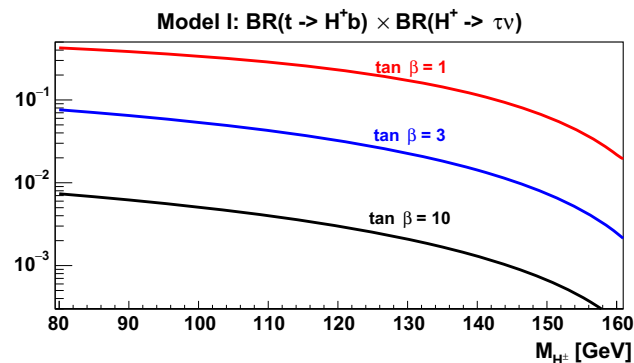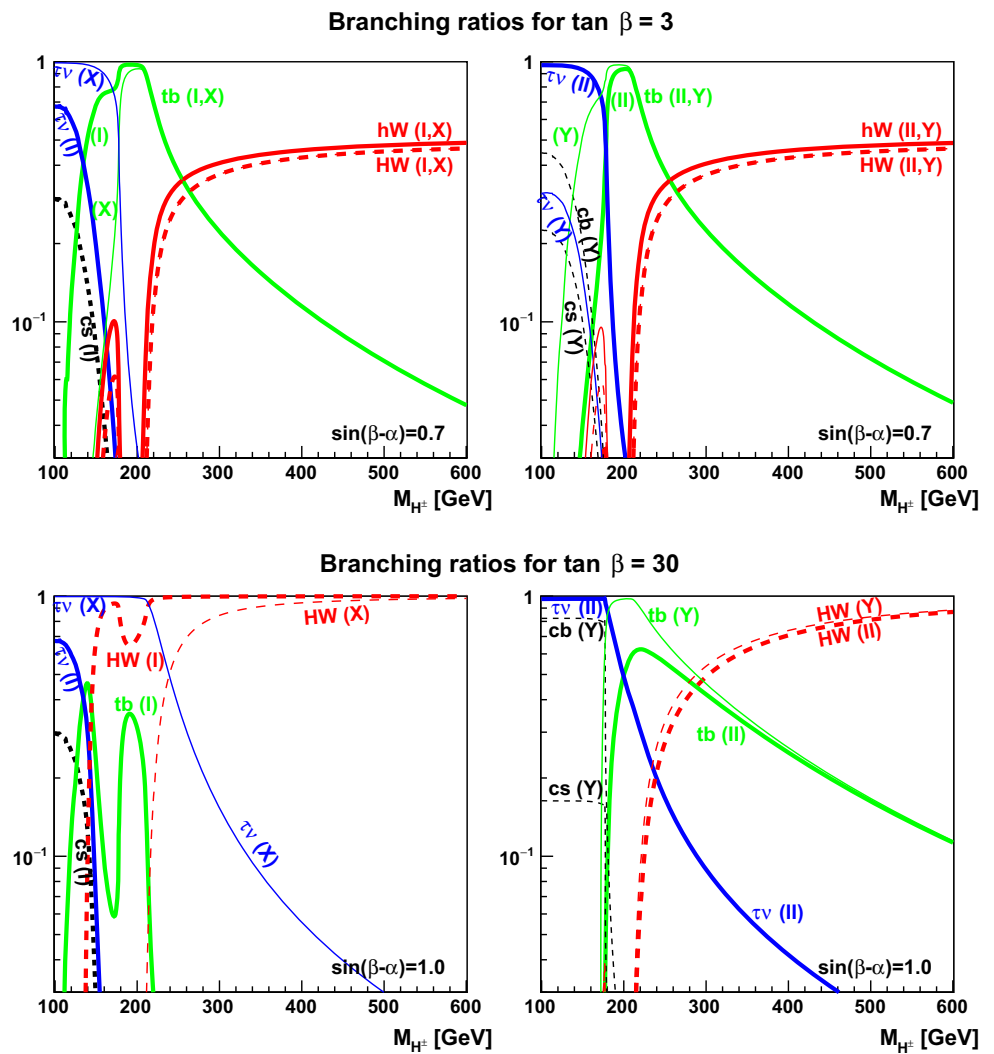


**Model I: BR(t -> H⁺b) × BR(H⁺ -> τν)**



**Fig. 5** Product of branching ratios, BR($t \rightarrow H^+b$) × BR($H^+ \rightarrow \tau^+\nu$), for Model I, and three values of $\tan\beta$, as indicated

which is closely approached by the LHC data on the Higgs–gauge–boson coupling, the $H^+H_1W^+$ coupling actually vanishes.

Hence, the $H^+ \rightarrow H_1W^+$ decay crucially depends on *some deviation from this limit*. We note that the $VVH_1$ cou-

pling is proportional to $\cos\alpha_2\cos(\beta - \alpha_1)$. Thus, the deviation of the square of this coupling from unity (which represents the SM-limit) is given by Eq. (5.8). Note that the experimental constraint (on the deviation of the coupling squared from unity) is 15–20% at the 95% CL [3,4].

For comparison, a recent study of decay modes that explicitly exhibit CP violation in Model II [60], compatible with all experimental constraints, considers $\tan\beta$ values in the range 1.3 to 3.3, with parameter points displaced from the alignment limit by $\sqrt{(\Delta\alpha_1/\pi)^2 + (\Delta\alpha_2/\pi)^2}$ ranging from 1.5 to 83.2% (the one furthest away has a negative value of $\alpha_1$).

This decay channel is also interesting for Model I [61].

## 6 $H^+$ production mechanisms at the LHC

This section describes $H^+$ production and detection channels at the LHC. Since a charged Higgs boson couples to mass, it will predominantly be produced in connection with heavy fermions, $\tau$, $c$, $b$ and $t$, or bosons, $W^\pm$ or $Z$, and likewise

**Fig. 6** Relative partial width for $H^+ \to H_1 W^+$, given by Eq. (5.8), vs. $\alpha_1$ and $\alpha_2$, for $\tan\beta = 1$ and 2. The *white* "*circles*" outline the region within which the $VVH_1$ coupling *squared* deviates by at most 10 or 30% from the SM value
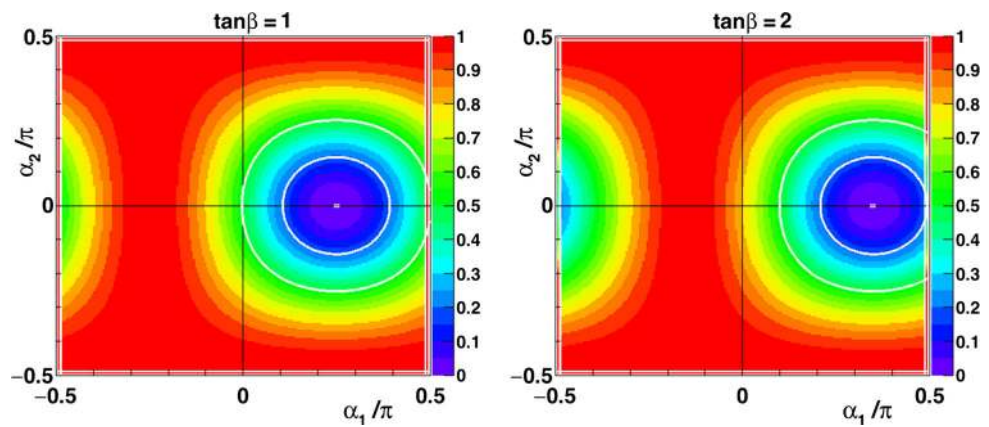
for the decays. The cross sections given here, are for illustration only. For the studies presented in Sects. 8–10 they are calculated independently.

We shall here split the discussion of possible $H^+$ production mechanisms into two mass regimes, according to whether the charged Higgs boson can be produced (in the on-shell approximation) in a top decay or whether it could decay to a top and a bottom quark. These two mass regimes will be referred to as "low" and "high" $M_{H^\pm}$ mass, respectively.

While discussing such processes in hadron–hadron collisions one should be aware that there are two approaches to the treatment of heavy quarks in the initial state. One may take the heavy flavors as being generated from the gluons, then the relevant number of active quarks is $N_f = 4$ (or sometimes 3). Alternatively, the $b$-quark can be included as a constituent of the hadron, then an $N_f = 5$ parton density should be used in the calculation of the corresponding cross section. These two approaches are referred to as the 4-flavor and 5-flavor schemes, abbreviated 4FS and 5FS. This should be kept in mind when referring to the lists of possible subprocesses initiated by heavy quarks and the corresponding figures in the following discussion. Below, we will use the notation $q'$, $Q$ and $Q'$ to denote quarks which are not $b$-quarks. We only indicate $b$-quarks when they couple to Higgs bosons, thus enhancing the rate.

For some discussions it is useful to distinguish "bosonic" and "fermionic" production mechanisms, since the former, corresponding to final states involving only $H^+$ and $W^-$, may proceed via an intermediate neutral Higgs, and thus depend strongly on its mass; see, e.g., Ref. [62].

## 6.1 Production processes

Below, we list all important $H^+$ production processes represented in Figs. 11, 12, 13, and 14 in the 5FS.[4]

### 6.1.1 Single $H^+$ production

A single $H^+$ can be accompanied by a $W^-$ (Fig. 7a, "bosonic") [63–71]:

$$gg \to W^- H^+, \tag{6.1a}$$
$$b\bar{b} \to W^- H^+, \tag{6.1b}$$

or by a $W^-$ and a $b$ jet (Fig. 7b, "fermionic") [72–86]:[5]

$$g\bar{b} \, (\to \bar{t} H^+) \to \bar{b} W^- H^+. \tag{6.2}$$

The pioneering study [63] of the bosonic process (6.1) already discussed both the triangle and the box contributions to the one-loop $gg$-initiated production, but considered massless $b$-quarks, i.e., the $b$-quark Yukawa couplings were omitted. This was subsequently restored in a complete one-loop calculation of the $gg$-initiated process [64,66], and it was realized that there can be a strong cancellation between the triangle and box diagrams. This interplay of triangle and box diagrams has also been explored in the MSSM [67].

NLO QCD corrections to the $b\bar{b}$-initiated production process were found to reduce the cross section by $\mathcal{O}\,(10\text{–}30\%)$ [68]. On the other hand, possible $s$-channel resonant production via heavier neutral Higgs bosons (see Fig. 7a (i) and (iii)) was seen to provide possible enhancements of up to two orders of magnitude [69]. These authors also pointed out that one should use running-mass Yukawa couplings, an effect which significantly reduced the cross section at high mass [70].

A first comparison of the $H^+ \to t\bar{b}$ signal with the $t\bar{t}$ background [65] (in the context of the MSSM) concluded that the signal could not be extracted from the background. More optimistic conclusions were reached for the $H^+ \to \tau^+ \nu$ channel [70,71], again in the context of the MSSM.

---

[4] Charge-conjugated processes are not shown separately. Higgs radiation from initial-state quarks is not shown explicitly.

[5] Note that in the 5FS (6.2) can be a tree-level process, whereas (6.1a) can not.

**Fig. 7** Feynman diagrams for the production processes (6.1) and (6.2)
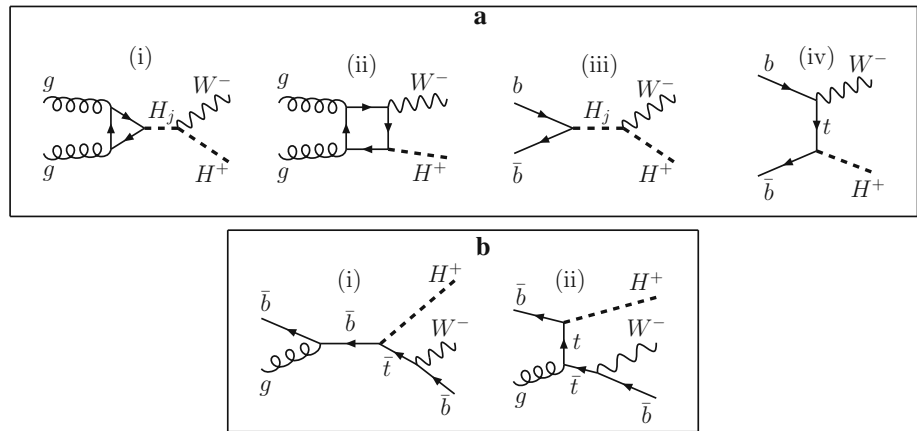


**Fig. 8** Feynman diagrams for the production processes (6.3)
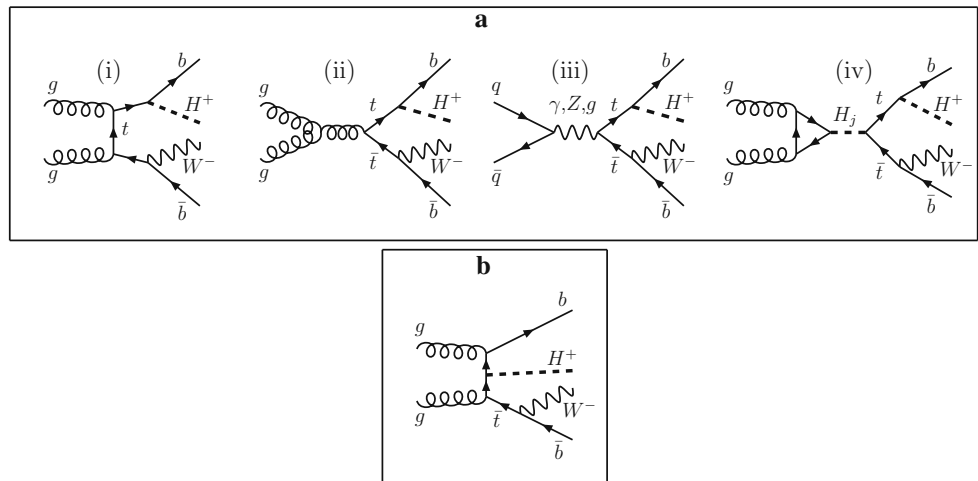


The first study [72] of the fermionic process (6.2) pointed out that there is a double counting issue (see Sect. 6.1.2). Subsequently, it was realized [73,87] that the $g\bar{b} \rightarrow H^+\bar{t}$ process could be described as $gg \rightarrow H^+\bar{t}b$, where a gluon splits into $b\bar{b}$ and one of these is not observed. As mentioned above, this approach is in the recent literature referred to as the four-flavor scheme (4FS) whereas in the five-flavor scheme (5FS) one considers $b$-quarks as proton constituents.

NLO QCD corrections to the $g\bar{b} \rightarrow H^+\bar{t}$ cross section have been calculated [77,78,86], and the resulting scale dependence studied [78,79], both in the 5FS and the 4FS. In a series of papers by Kidonakis [80,82,85], soft-gluon corrections have been included at the "approximate NNLO" order and found to be significant near threshold, i.e., for heavy $H^+$. A recent study [86] is devoted to total cross sections in the intermediate-mass region, $M_{H^+} \sim m_t$, providing a reliable interpolation between low and high masses.

These fixed-order cross section calculations have been merged with parton showers [81,83,84,88], both at LO and NLO, in the 4FS and in the 5FS. The 5FS results are found to exhibit less scale dependence [84].

Different background studies [74–76] compared triple $b$-tagging vs. 4-$b$-tagging, identifying parameter regions where either is more efficient.

In addition to the importance of the $t\bar{t}$ channel at low mass, the following processes containing two accompanying $b$ jets (see Fig. 8) are important at high charged-Higgs mass:

$$gg, q\bar{q}, b\bar{b} (\rightarrow t\bar{t} \rightarrow b\bar{t}H^+) \rightarrow b\bar{b}W^-H^+, \tag{6.3a}$$
$$gg, q\bar{q} (\rightarrow b\bar{t}H^+) \rightarrow b\bar{b}W^-H^+. \tag{6.3b}$$

There are also processes with a single $H^+$ and two jets (see Fig. 9):
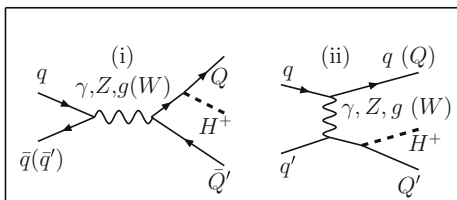
$$\text{(i): } q\bar{q}(\bar{q}') \rightarrow Q\bar{Q}'H^+, \quad \text{(ii): } qq' \rightarrow q(Q)Q'H^+. \tag{6.4}$$

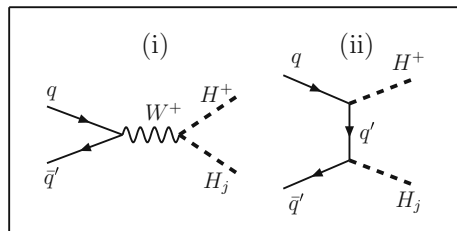In this particular case, with many possible gauge boson couplings, one of the final-state jets could be a $b$.

In addition, single $H^+$ production can be initiated by a $b$-quark,
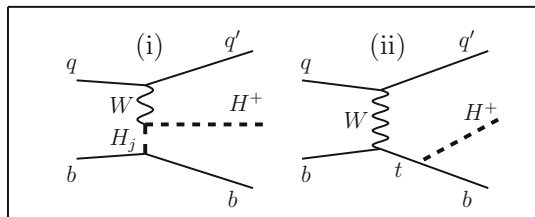
$$qb \rightarrow q'H^+b, \tag{6.5}$$
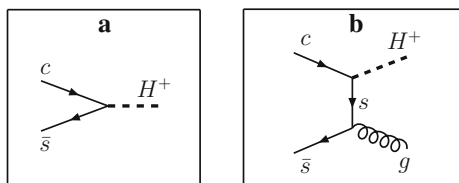
as illustrated in Fig. 10.

**Fig. 9** Feynman diagrams for the production processes (6.4). If the line has no arrow, it represents either a quark or an antiquark



**Fig. 10** Feynman diagrams for the production processes (6.5)



**Fig. 11** Feynman diagrams for the production processes (6.6)

In the 5FS, single $H^+$ production can also take place from $c$ and $s$ quarks, typically accompanied by a gluon jet [89–92] (Fig. 11):

$$c\bar{s} \rightarrow H^+, \tag{6.6a}$$
$$c\bar{s} \rightarrow H^+ g. \tag{6.6b}$$

Similarly, one can consider $c\bar{b}$ initial states.

At infinite order the 4FS and the 5FS should only differ by terms of $\mathcal{O}(m_b)$, but the perturbation series of the two schemes are organized differently. Some authors (see, e.g., Ref. [83]) advocate combining the two schemes according to the "Santander matching" [93]:

$$\sigma = \frac{\sigma(4\text{FS}) + w\sigma(5\text{FS})}{1 + w}, \tag{6.7}$$

with the relative weight factor

$$w = \log \frac{M_{H^\pm}}{m_b} - 2, \tag{6.8}$$

since the difference between the two schemes is logarithmic, and in the limit of $M_{H^\pm} \gg m_b$ the 5FS should be exact.



**Fig. 12** Feynman diagrams for the production processes (6.9)

### 6.1.2 The double counting and NWA issues

A $b$-quark in the initial state may be seen as a constituent of the proton (5FS), or as resulting from the gluon splitting into $b\bar{b}$ (4FS). Adding $gg \rightarrow b\bar{b}g \rightarrow bH^+\bar{t}$ (with one $b$ possibly not detected) and $g\bar{b} \rightarrow H^+\bar{t}$ in the 5FS one may therefore commit double counting [94,95]. The resolution lies in subtracting a suitably defined infrared-divergent part of the gluon-initiated amplitude [88].[6] The problem can largely be circumvented by choosing either the 5FS or the 4FS. For a more pragmatic approach, see Refs. [97,98].

A related issue is the one of low-mass $H^+$ production via $t$-quark decay, $gg, q\bar{q} \rightarrow t\bar{t}$ followed by $t \rightarrow H^+b$ (with $\bar{t}$ a spectator), usually treated in the Narrow Width Approximation (NWA). The NWA, however, fails the closer the top and charged Higgs masses are, in which case the finite top width needs to be accounted for, which in turn implies that the full gauge invariant set of diagrams yielding $gg, q\bar{q} \rightarrow H^+b\bar{t}$ has to be computed. A considerable effort has been made to understand this implementation; see also Refs. [99–101].

### 6.1.3 $H^+H_j$ and $H^+H^-$ production

We can have a single $H^+$ production in association with a neutral Higgs boson $H_j$ [102–107]:

$$q\bar{q}' \rightarrow H^+ H_j, \tag{6.9}$$

as shown in Fig. 12.

For $H^+H^-$ pair production we have [108–118]:

$$gg, q\bar{q}, b\bar{b} \rightarrow H^+ H^-, \tag{6.10a}$$
$$q\bar{q}(\bar{q}'), qQ \rightarrow q'Q'H^+ H^-, \tag{6.10b}$$

as illustrated in Figs. 13 and 14, respectively. These mechanisms would be important for light charged Higgs bosons, as allowed in Models I and X.

---

[6] For a complete discussion of the flavor scheme choice in inclusive charged Higgs production associated with fermions see IV.3.2 of [96] and references therein.
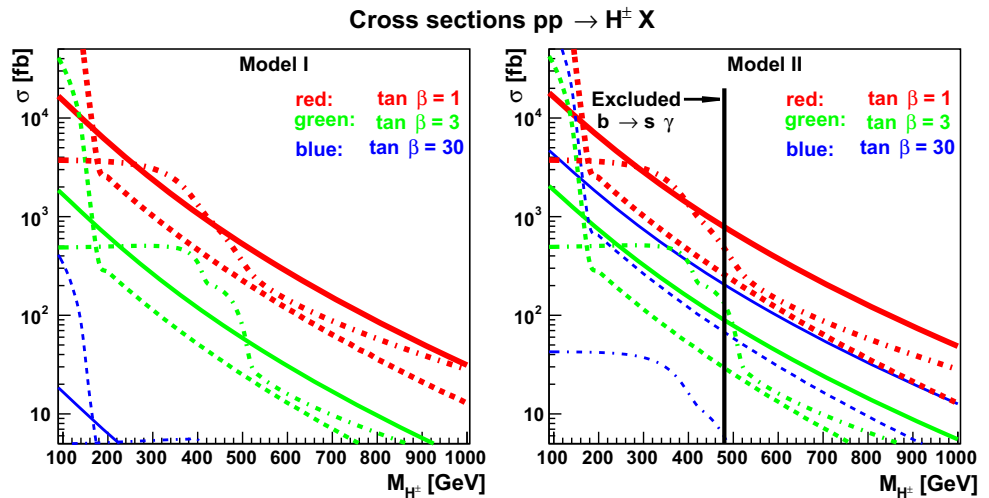
**Fig. 13** Feynman diagrams for the pair production processes (6.10a)
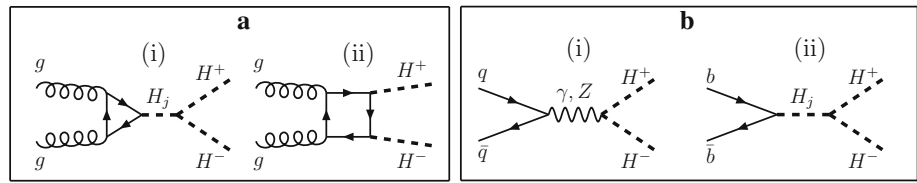


**Fig. 14** Feynman diagrams for the pair production processes (6.10b)
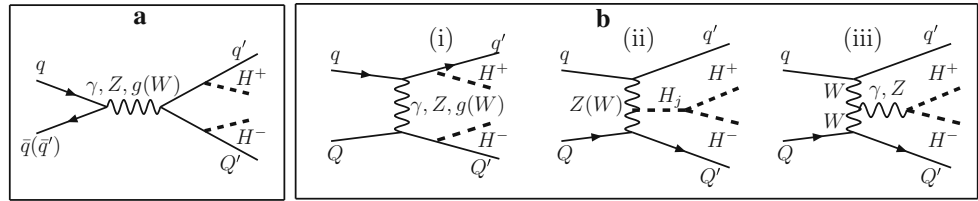


**Fig. 15** Charged Higgs production cross sections in the 2HDM, at 14 TeV. *Left* Model I (or X). *Right* Model II (or Y). *Solid and dotted curves* refer to "fermionic" channels, whereas *dash-dotted* refer to "bosonic" ones (see text)



## 6.2 Production cross sections

In this section, predictions for single Higgs production at 14 TeV for the CP-conserving 2HDM, Models I and II (valid also for X and Y) are discussed.

In Fig. 15, $pp \to H^+X$ cross sections for the main production channels are shown at leading order, sorted by the parton-level mechanism [62].[7] The relevant partonic channels can be categorized as:

- "fermionic": $g\bar{b} \to H^+\bar{t}$, Fig. 7 **b** (solid),
- "fermionic": $gg \to H^+b\bar{t}$, Fig. 8 **a**, **b** (dotted),
- "bosonic": $gg \to H_j \to H^+W^-$, Fig. 7 **a** (i) (dash-dotted).

The charge-conjugated channels are understood to be added unless specified otherwise. No constraints are imposed here, neither from theory (like positivity, unitarity), nor from experiments.

The CTEQ6L (5FS) parton distribution functions [119] are adopted here, with the scale $\mu = M_H$. Three values of $\tan\beta$ are considered, and $M_H$ and $M_A$ are held fixed at $(M_H, M_A) = (500, 600)$ GeV. Furthermore, we consider the CP-conserving alignment limit, with $\sin(\beta - \alpha) = 1$. The bosonic cross section is accompanied by a next-to-leading order QCD $K$-factor enhancement [120].

Several points are worth mentioning:

- To any contribution at fixed order in the perturbative expansion of the gauge coupling, the three cross sections are to be merged with regards to the interpretation in different flavor schemes, as discussed above. In the following, we focus on the first fermionic channel in the 5FS at tree level.
- The enhancement exhibited by the dotted curve at low masses is due to resonant production of $t$-quarks which decay to $H^+b$. However, in Model I this mode is essentially excluded by LHC data (see Sect. 7.2.4), and in Model II it is excluded by the $B \to X_s\gamma$-constraint (see Sect. 7.1.2).
- Model I differs from Model II also for $\tan\beta = 1$, because of a different relative sign between the Yukawa couplings

---

[7] In the Feynman diagrams $t$ is represented by its dominant decay products $W^+b$.
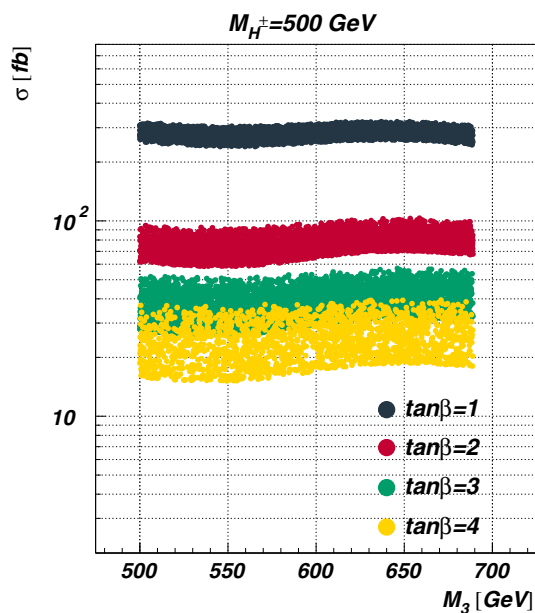
**Fig. 16** Charged Higgs bosonic production cross sections in the 2HDM, Model II, for 14 TeV, and a fixed value of $M_{H^\pm} = 500$ GeV, plotted vs. $M_3 \equiv M_A$ for $\tan \beta = 1, 2, 3$ and 4

proportional to $m_t$ and those proportional to $m_b$; see Table 6.

- Models X and Y will have the same production cross sections as Models I and II, respectively, but the sensitivity in the $\tau\nu$-channel would be different.
- The bumpy structure seen for the bosonic mode is due to resonant production of neutral Higgs bosons, and it depends on the values of $M_H$ and $M_A$. Note that in the MSSM the masses of the heavier neutral Higgs bosons are close to that of the charged one, and this resonant behavior is absent.

While recent studies (see Sect. 6.1.1) provide a more accurate calculation of the $g\bar{b} \to H^+\bar{t}$ cross section than what is given here, they typically leave out the 2HDM model-specific $s$-channel (possibly resonant) contribution to the cross section.

In Fig. 16, the bosonic charged-Higgs production cross section vs. $M_3 \equiv M_A$ for a set of CP-conserving parameter points that satisfy the theoretical and experimental constraints [62] (see also [121,122]) are presented. These are shown in different colors for different values of $\tan \beta$. The spread in cross section values for each value of $\tan \beta$ and $M_A$ reflects the range of allowed values of the other parameters scanned over, namely $\mu$, $M_H$ and $\alpha$.

Low values of $\tan \beta$ are enhanced for the bosonic mode due to the contribution of the $t$-quark in the loop, whereas the modulation is due to resonant $A$ production. In the CP-violating case, this modulation is more pronounced [62].

As summarized by the LHC Top Physics Working Group the $pp \to t\bar{t}$ cross section has been calculated at next-to-next-to leading order (NNLO) in QCD including resummation of next-to-next-to-leading logarithmic (NNLL) soft-gluon terms with the software Top++2.0 [123–129]. The decay width $\Gamma(t \to bW^+)$ is available at NNLO [130–136], while the decay width $\Gamma(t \to bH^+)$ is available at NLO [137].

## 7 Experimental constraints

Here we review various experimental constraints for charged Higgs bosons derived from different low (mainly $B$-physics) and high (mainly LEP, Tevatron and LHC) energy processes. Also some relevant information on the neutral Higgs sector is presented. Some observables depend solely on $H^+$ exchange, and are thus independent of CP violation in the potential, whereas other constraints depend on the exchange of neutral Higgs bosons, and are sensitive to the CP violation introduced via the mixing discussed in Sect. 2.2. Due to the possibility of $H^+$, in addition to $W^+$ exchange, we are getting constraints from a variety of processes, some at tree and some at the loop level. In addition, we present general constraints coming from electroweak precision measurements, $S$, $T$, the muon magnetic moment and the electric dipole moment of the electron. The experimental constraints listed below are valid only for Model II, if not stated otherwise.[8] Also, some of the constraints are updated, with respect to those used in the studies presented in later sections.

The charged-Higgs contribution may substantially modify the branching ratios for $\tau\nu_\tau$-production in $B$-decays [140]. An attempt to describe various $\tau$ and $B$ anomalies (also $W \to \tau\nu$) in the 2HDM, Model III, with a novel ansatz relating up- and down-type Yukawa couplings, can be found in [141]. This analysis points towards an $H^+$ mass around 100 GeV, with masses of other neutral Higgs bosons in the range 100–125 GeV. A similar approach to describe various low-energy anomalies by introducing additional scalars can be found in [142]. Here, a lepton-specific 2HDM (i.e., of type X) with non-standard Yukawa couplings has been analyzed with the second neutral CP-even Higgs boson light (below 100 GeV) and a relatively light $H^+$, with a mass of the order of 200 GeV.

### 7.1 Low-energy constraints

As mentioned above, several decays involving heavy-flavor quarks could be affected by $H^+$ in addition to $W^+$-exchange. Data on such processes provide constraints on the coupling

---

[8] Analyses with general Yukawa couplings can be found in Refs. [138, 139].

(represented by tan $\beta$) and the mass, $M_{H^\pm}$. Below, we discuss the most important ones.

### 7.1.1 Constraints from $H^+$ tree-level exchange

**$B \to \tau\nu_\tau(X)$**: The measurement of the branching ratio of the inclusive process $B \to \tau\nu_\tau X$ [143] leads to the following constraint, at the 95% CL:

$$\frac{\tan \beta}{M_{H^\pm}} < 0.53 \text{ GeV}^{-1}. \tag{7.1}$$

This is in fact a very weak constraint (a similar result can be obtained from the leptonic tau decays at tree level [144]). A more recent measurement for the exclusive case gives BR($B \to \tau\nu_\tau$) = $(1.14 \pm 0.27) \times 10^{-4}$ [145].[9] With a Standard Model prediction of $(0.733 \pm 0.141) \times 10^{-4}$ [147],[10] we obtain

$$r_{H \text{ exp}} = \frac{\text{BR}(B \to \tau\nu_\tau)}{\text{BR}(B \to \tau\nu_\tau)_{\text{SM}}} = 1.56 \pm 0.47. \tag{7.2}$$

Interpreted in the framework of the 2HDM at tree level, one finds [148–150]

$$r_{H \text{ 2HDM}} = \left[ 1 - \frac{m_B^2}{M_{H^\pm}^2} \tan^2 \beta \right]^2. \tag{7.3}$$

Two sectors of the ratio tan $\beta/M_{H^\pm}$ are excluded. Note that this exclusion is relevant for high values of tan $\beta$.

**$B \to D\tau\nu_\tau$**: The ratios [151]

$$R^{\text{exp}}(D^{(*)}) = \frac{\text{BR}(B \to D^{(*)}\tau\nu_\tau)}{\text{BR}(B \to D^{(*)}\ell\nu_\ell)}, \quad \ell = e, \mu, \tag{7.4}$$

are sensitive to $H^+$-exchange, and they lead to constraints similar to the one following from $B \to \tau\nu_\tau X$ [152]. In fact, there has been some tension between BaBar results [151,153,154] and both the 2HDM (II) and the SM. These ratios have also been measured by Belle [155,156] and LHCb [157]. Recent averages [141,158] are summarized in Table 2, together with the SM predictions [159–161]. They are compatible at the $2\sigma$–$3\sigma$ level. A comparison with the 2HDM (II) concludes [155] that the results are compatible for tan $\beta/M_{H^\pm}$ = 0.5/GeV. However, in view of the high values for $M_{H^\pm}$ required by the $B \to X_s\gamma$ constraint, uncomfortably high values of tan $\beta$ would be required. The studies

---

[9] The error of the $B \to \tau\nu$ measurement, given by HFAG [146] and released after the PDG 2014 [145], is slightly lower: $(1.14 \pm 0.22) \times 10^{-4}$.

[10] We have added in quadrature symmetrized statistical and systematic errors.

**Table 2** Average experimental values [141,158] and SM predictions [141,142,159–161]

| Ratio | Experiment | SM |
|---|---|---|
| $R(D^*)$ | $0.321 \pm 0.021$ | $0.252 \pm 0.005$ |
| $R(D)$ [158] | $0.388 \pm 0.047$ | $0.300 \pm 0.010$ |
| $R(D)$ [141] | $0.408 \pm 0.050$ | $0.297 \pm 0.017$ |

given for Model II in Sect. 8.3 do not take this constraint into account.

**$D_s \to \tau\nu_\tau$**: Severe constraints can be obtained, which are competitive with those from $B \to \tau\nu_\tau$ [162].

### 7.1.2 Constraints from $H^+$ loop-level exchange

**$B \to X_s\gamma$**: The $B \to X_s\gamma$ transition may also proceed via charged Higgs-boson exchange, which is sensitive to the values of tan $\beta$ and $M_{H^\pm}$. The allowed region depends on higher-order QCD effects. A huge effort has been made devoted to the calculation of these corrections, the bulk of which are the same as in the SM [164–183]. They are now complete up to NNLO order. On top of these, there are 2HDM-specific contributions [13,184–188] that depend on $M_{H^\pm}$ and tan $\beta$. The result is that mass roughly up to $M_{H^\pm} = 480$ GeV is excluded for high values of tan $\beta$ [13], with even stronger constraints for very low values of tan $\beta$. Recently, a new analysis [189] of Belle results [190] concludes that the lower limit is 540 GeV. Also note the new result of Misiak and Steinhauser [14] with lower limit in the range 570–800 GeV; see Fig. 17 (right) for high tan $\beta$ and high $H^+$ masses. We have here adopted the more conservative value of 480 GeV, however, our results can easily be re-interpreted for this new limit. Constraints from $B \to X_s\gamma$ decay for lower $H^+$ masses are presented in Fig. 19 together with other constraints.

For low values of tan $\beta$, the constraint is even more severe. This comes about from the charged-Higgs coupling to $b$ and $t$ quarks ($s$ and $t$) containing terms proportional to $m_t/\tan\beta$ and $m_b \tan\beta$ ($m_s \tan\beta$). The product of these two couplings determine the loop contribution, where there is an intermediate $tH^-$ state, and leads to terms proportional to $m_t^2/\tan^2\beta$ (responsible for the constraint at low tan $\beta$) and $m_t m_b$ (responsible for the constraint that is independent of tan $\beta$). For Models I and X, on the other hand, both these couplings are proportional to cot $\beta$. Thus, the $B \to X_s\gamma$ constraint is in these models only effective at low values of tan $\beta$.[11] This can be seen in Figs. 17 (left) and 18, where the new results from the $B \to X_s\gamma$ analysis applied to Model I of the 2HDM are shown. We stress that Model I can avoid the $B \to X_s\gamma$ constraints and hence it can accommodate a light $H^+$.
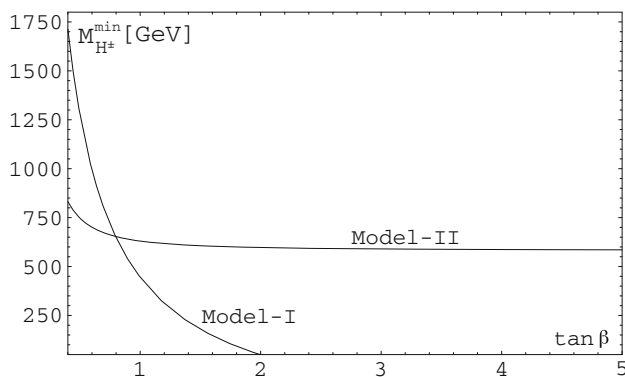
---

[11] For early studies, see [15,191].
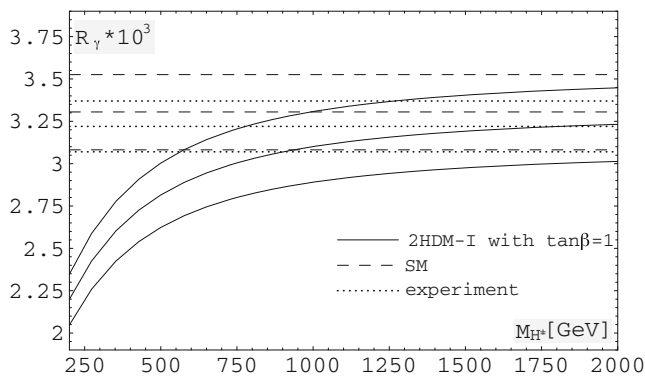
**Fig. 17** $BR(B^- \to X_s\gamma)$ as a function of $M_{H^\pm}$ for Model I (*left*) and Model II (*right*), at two values of $\tan\beta$. *Solid* and *dashed lines* correspond to the NNLO 2HDM and SM predictions, respectively. (Shown
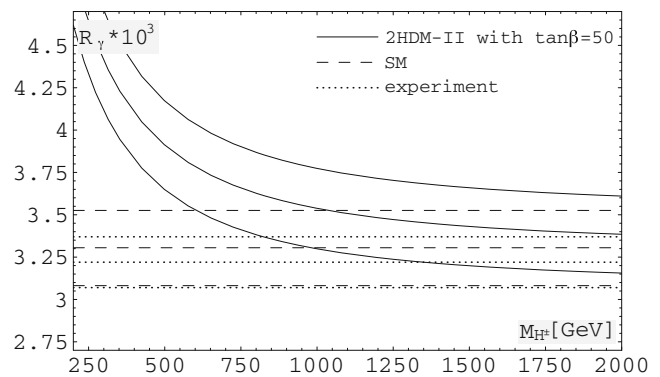
are central values with $\pm 1\sigma$ shifts.) *Dotted curves* represent the experimental average. (Reprinted with kind permission from the authors, Fig. 2 of [14])



**Fig. 18** 2HDM 95%C.L. $B \to X_s\gamma$ exclusion (*lower part*) in the plane of $\tan\beta$ and $M_{H^\pm}$. (Reprinted with kind permission from the authors, Fig. 4 of [14])

**$B_0$–$\bar{B}_0$ mixing:** Due to the possibility of charged-Higgs exchange, in addition to $W^+$ exchange, the $B_0$–$\bar{B}_0$ mixing constraint excludes low values of $\tan\beta$ (for $\tan\beta < \mathcal{O}(1)$) and low values of $M_{H^\pm}$ [192–197]. Recent values for the oscillation parameters $\Delta m_d$ and $\Delta m_s$ are given in Ref. [198], only at very low values of $\tan\beta$ do they add to the constraints coming from $B \to X_s\gamma$.

### 7.1.3 Other precision constraints

**$T$ and $S$:** The precisely measured electroweak (oblique) parameters $T$ and $S$ correspond to radiative corrections, and are (especially $T$) sensitive to the mass splitting of the additional scalars of the theory. In papers [47,48] general expressions for these quantities are derived for the MHDMs and by confronting them with experimental results, in particular $T$, strong constraints are obtained on the masses of scalars. In general, $T$ imposes a constraint on the splitting in the scalar sector, a mass splitting among the neutral scalars gives a negative contribution to $T$, whereas a splitting between the charged and neutral scalars gives a positive contribution. A

recent study [199] also demonstrates how RGE running may induce contributions to $T$ and $S$. Current data on $T$ and $S$ are given in [145].

**The muon anomalous magnetic moment:** We are here considering heavy Higgs bosons ($M_1$, $M_{H^\pm} \gtrsim 100\,\text{GeV}$), with a focus on the Model II, therefore, according to [39,200,201], the 2HDM contribution to the muon anomalous magnetic moment is negligible even for $\tan\beta$ as high as $\sim 40$ (see, however, [202]).

**The electron electric dipole moment:** The bounds on electric dipole moments constrain the allowed amount of CP violation of the model. For the study of the CP-non-conserving Model II presented in Sect. 8.3, the bound [203] (see also [204]):

$$|d_e| \lesssim 1 \times 10^{-27}[e\,\text{cm}], \tag{7.5}$$

was adopted at the $1\sigma$ level (More recently, an order-of-magnitude stronger bound has been established [205]). The contribution due to neutral Higgs exchange, via the two-loop Barr–Zee effect [206], is given by Eq. (3.2) of [204].

### 7.1.4 Summary of low-energy constraints

A summary of constraints of the 2HDM Model II coming from low-energy physics performed by the "Gfitter" group [207] is presented in Fig. 19. The more recent inclusion of higher-order effects pushes the $B \to X_s\gamma$ constraint up to around 480 GeV [13] or even higher, as discussed above. See also Refs. [198,208,209].

### 7.2 High-energy constraints

Most bounds on charged Higgs bosons are obtained in the low-mass region, where a charged Higgs might be produced in the decay of a top quark, $t \to H^+ b$, with the
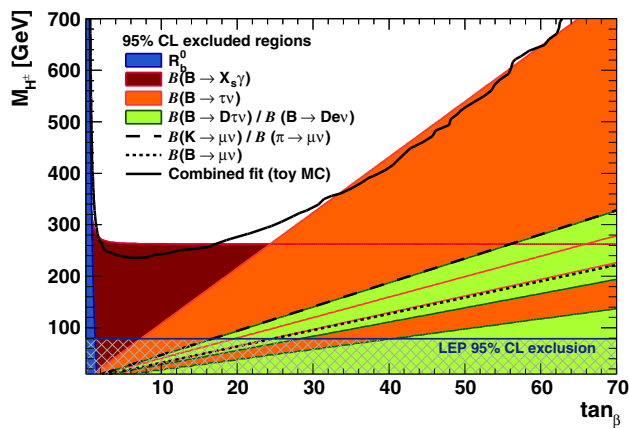
**Fig. 19** Model II 95% CL exclusion regions in the $(\tan\beta, M_{H^\pm})$ plane. (Reprinted with kind permission from EPJC and the authors of "Gfitter" [207]). A new analysis, including the updated bound from $B \to X_s\gamma$, is being prepared by the "Gfitter" group

$H^+$ subsequently decaying according to Eqs. (5.1a–c), (5.2) or (5.3). Of special interest are the decays $H^+ \to \tau^+\nu$ and $H^+ \to c\bar{s}$. For comparison with data, products like $BR(t \to H^+b) \times BR(H^+ \to \tau^+\nu)$ are relevant, as presented in Sect. 5.3. At high charged-Higgs masses, the $HW$ rate can be important (if kinematically open). On the other hand, the $hW$ channel can dominate over $HW$, because of the larger phase space. However, as illustrated in Fig. 4, it vanishes in the alignment limit.

### 7.2.1 Charged-Higgs constraints from LEP

The branching ratio $R_b \equiv \Gamma_{Z \to b\bar{b}}/\Gamma_{Z \to \mathrm{had}}$ would be affected by Higgs exchange. Experimentally $R_b = 0.21629 \pm 0.00066$ [145]. The contributions from neutral Higgs bosons to $R_b$ are negligible [22], however, charged Higgs-boson contributions are given by [210], Eq. (4.2), exclude low values of $\tan\beta$ and low $M_{H^\pm}$. See also Fig. 19.

LEP and the Tevatron have given limits on the mass and couplings, for charged Higgs bosons in the 2HDM. At LEP a lower mass limit of 80 GeV that refers to the Model II scenario for $BR(H^+ \to \tau^+\nu) + BR(H^+ \to c\bar{s}) = 100\%$ was derived. The mass limit for $BR(H^+ \to \tau^+\nu) = 100\%$ is 94 GeV (95% CL), and for $BR(H^+ \to c\bar{s}) = 100\%$ the region below 80.5 as well as the region 83–88 GeV are excluded (95% CL). Search for the decay mode $H^+ \to AW^+$ with $A \to b\bar{b}$, which is not negligible in Model I, leads to the corresponding $M_{H^\pm}$ limit of 72.5 GeV (95% CL) if $M_A > 12$ GeV [17].

### 7.2.2 Search for charged Higgs at the Tevatron

A D0 analysis [211] with an integrated luminosity 1 fb$^{-1}$ has been performed for $t \to H^+b$, with $H^+ \to c\bar{s}$ and $H^+ \to \tau^+\nu$. In the SM one has $BR(t \to W^+b) = 100\%$ with $W \to$

$l\nu/q'\bar{q}$. The presence of a sizable $BR(t \to H^+b)$ would change these ratios. For the optimum case of $BR(H^+ \to q'\bar{q}) = 100\%$, upper bounds on $BR(t \to H^+b)$ between 19 and 22% were obtained for 80 GeV $< M_{H^\pm} < 155$ GeV. In [211] the decay $H^+ \to q'\bar{q}$ was assumed to be entirely $H^+ \to c\bar{s}$. But these limits on $BR(t \to H^+b)$ also apply to the case of both $H^+ \to c\bar{s}$ and $H^+ \to c\bar{b}$ having sizable BRs, as discussed in [212]. This is because the search strategy merely requires that $H^+$ decays to quark jets.

An alternative strategy was adopted in the CDF analysis [213] with an integrated luminosity 2.2 fb$^{-1}$. A direct search for the decay $H^+ \to q'\bar{q}$ was performed by looking for a peak centered at $M_{H^\pm}$ in the di-jet invariant mass distribution, which would be distinct from the peak at $M_W$ arising from the SM decay $t \to W^+b$ with $W \to q'\bar{q}$. For the optimum case of $BR(H^+ \to q'\bar{q}) = 100\%$, upper bounds on $BR(t \to H^+b)$ between 32 and 8% were obtained for 90 GeV $< M_{H^\pm} < 150$ GeV. No limits on $BR(t \to H^+b)$ were given for the region 70 GeV $< M_{H^\pm} < 90$ GeV due to the large background from $W \to q'\bar{q}$ decays. For the region 60 GeV $< M_{H^\pm} < 70$ GeV, limits on $BR(t \to H^+b)$ between 9 and 12% were derived.

A search for charged-Higgs production has also been carried out by D0 [214] at higher masses, where $H^+ \to t\bar{b}$. Bounds on cross section times branching ratio have been obtained for Models I and III, in the range 180 GeV $\leq M_{H^\pm} \leq 300$ GeV, for $\tan\beta = 1$ and $\tan\beta > 10$.

### 7.2.3 LHC searches for charged Higgs

A search for $t \to H^+b$ followed by the decay $H^+ \to c\bar{s}$ at the LHC (7 TeV) has been performed by the ATLAS collaboration with 4.7 fb$^{-1}$ [217]. Assuming $BR(H^+ \to c\bar{s}) = 100\%$, the derived upper limits on $BR(t \to H^+b)$ are 5.1, 2.5 and 1.4% for $M_{H^\pm} = 90$ GeV, 110 GeV and 130 GeV, respectively. These limits are superior to those from the Tevatron search [213], and exclude a sizable region of the Yukawa-coupling plane,[12] not excluded by $B \to X_s\gamma$. The recent data from CMS [215] on the production in the $t\bar{t}$ channel of light charged Higgs bosons decaying to $c\bar{s}$ at the collision energy of 8 TeV and with an integrated luminosity 19.7 fb$^{-1}$ show no deviation from the SM. Assuming $BR(H^+ \to c\bar{s}) = 100\%$, the derived upper limits on $BR(t \to H^+b)$ are 1.2–6.5% for $M_{H^\pm}$ in the range (90–160 GeV); see Fig. 20. The data points are found to be consistent with the signal-plus-background hypothesis for a charged Higgs-boson mass of 150 GeV for a best-fit branching fraction value of $(1.2 \pm 0.2)\%$ including both statistical and systematic errors. The local observed significance is $2.4\sigma$ ($1.5\sigma$ including the look-elsewhere effect).
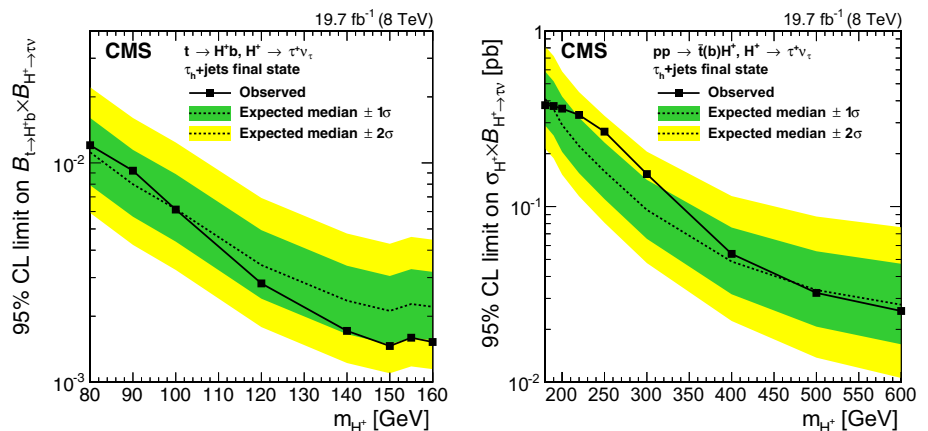
---

[12] See Sect. 9.1 for details.
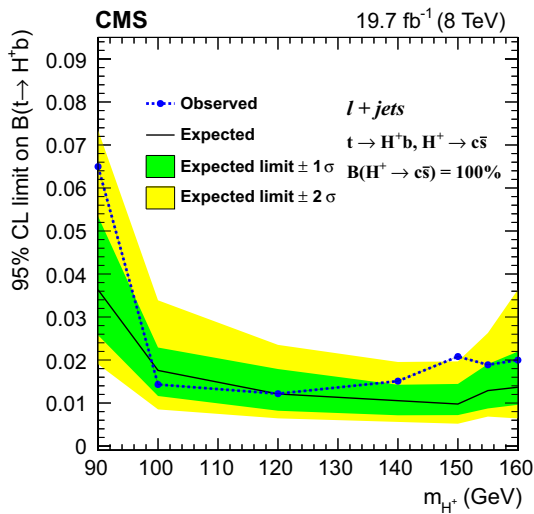
**Fig. 20** CMS exclusion limit on the branching fraction $BR(t \to H^+b)$ as a function of $M_{H^\pm}$ assuming $BR(H^+ \to c\bar{s}) = 100\%$. (Reprinted with kind permission from JHEP and the authors, Fig. 6 of [215])

Likewise, a search for a light charged Higgs boson produced in the decay $t \to H^+b$ and decaying to $\tau^+\nu$ has been performed by CMS [216,220]; see Fig. 21. For a charged Higgs-boson mass between 80 and 160 GeV, they obtain upper limits on the product of branching fractions $BR(t \to H^+b) \times BR(H^+ \to \tau^+\nu)$ in the range 0.23–1.3%.

Similarly, constraints are obtained by ATLAS [218] from the 8 TeV measurements at the LHC, with luminosity 19.5 fb$^{-1}$. Results for low- and high-mass $H^+$ are shown in Fig. 22, for $BR(t \to H^+b) \times BR(H^+ \to \tau^+\nu)$ (left) and for $\sigma(pp \to H^+t + X) \times BR(H^+ \to \tau^+\nu)$ (right), respectively.

In Fig. 23 (left) CMS results [216] for the case $BR(H^+ \to t\bar{b}) = 100\%$ are presented. Results of a recent ATLAS analysis, performed using a multi-jet final state for the process $gb \to tH^-$ are presented in Fig. 23 (right). An excess of

events above the background-only hypothesis is observed across a wide mass range, amounting to up to $2.4\sigma$.

In addition, ATLAS provides limits on the $s$-channel production cross section, via the decay mode $H^+ \to t\bar{b}$ for heavy charged Higgs bosons (masses from 0.4 TeV to 3 TeV), for two categories of final states; see Fig. 24.

It should be noted that in all these figures, "expectations" are a measure of the instrumental capabilities, and the amount of data. In fact, theoretical (model-dependent) expectations can be significantly lower. In particular, in Model I and Model II, the branching ratio for $H^+ \to \tau^+\nu$ is at high masses very low, see Fig. 4. Thus, these models are not yet constrained by the high-mass results shown in Figs. 21 and 22 [221]. However, for Model X the $\tau^+\nu$ branching ratio is sufficiently high for these searches to be already relevant.
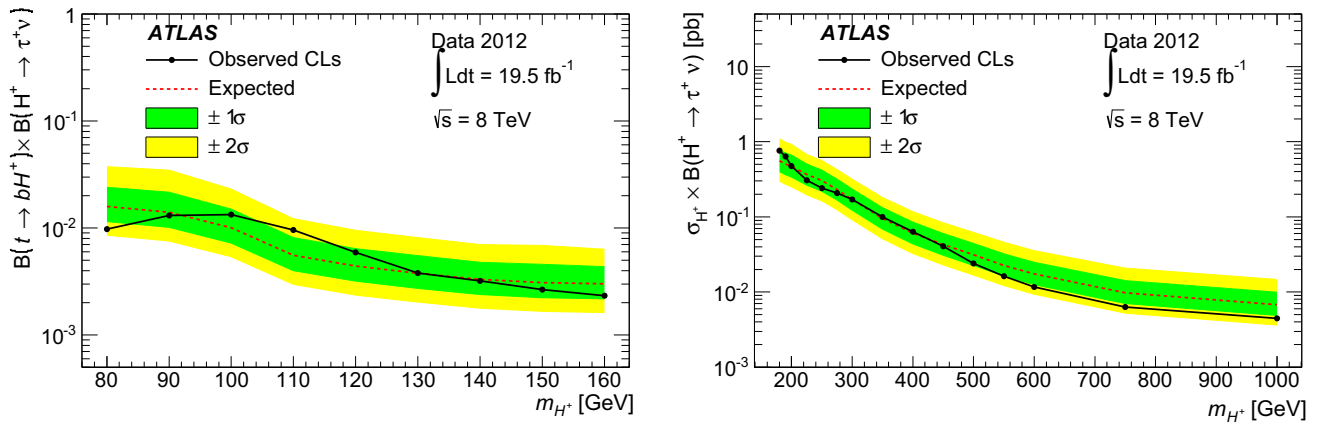
### 7.2.4 Summary of search for charged scalars at high energies

The LEP lower limits on the mass for light $H^+$ are 80.5–94 GeV, depending on the assumption on the $H^+$ decaying 100% into $c\bar{s}$, $b\bar{s}$ or $c\bar{s} + b\bar{s}$ channels.

For low-mass $H^+$, $\sim$80 (90)–160 GeV, limits for the top decay to $H^+b$ were derived at the Tevatron and the LHC (ATLAS and CMS) at the level of a few per cent (5.1–1.2%) for the assmption of 100% decay to $c\bar{s}$. CMS results on $BR(t \to H^+b) \times BR(H^+ \to \tau^+\nu)$ reached down to 1.3–0.23%.

For heavy $H^+$ the region between 200 and 600 GeV was studied at LHC for $\sigma(pp \to t(b)H^+) \times BR(H^+ \to \tau^+\nu)$. A special search for an $s$-channel resonance with mass of $H^+$ up to 3 TeV with the decay mode to $t\bar{b}$ was performed by ATLAS.

Some excesses at $2.4\sigma$ for $H^+$ mass equal to 150 GeV, as well as for masses between 220 and 320 GeV, are reported by CMS [215,216] and for a very wide $H^+$ mass range 200–600 GeV by ATLAS [219].

**Fig. 21** CMS model-independent upper limits on $BR(t \to H^+b) \times BR(H^+ \to \tau^+\nu_\tau)$ (*left*) and on $\sigma(pp \to t(b)H^+) \times BR(H^+ \to \tau^+\nu_\tau)$ (*right*). (Reprinted with kind permission from JHEP and the authors, Fig. 8 of [216])

**Fig. 22** ATLAS upper limits on the production and decay of low-mass (*left*) and high-mass (*right*) charged Higgs bosons. (Reprinted with kind permission from JHEP and the authors, Fig. 7 of [218])
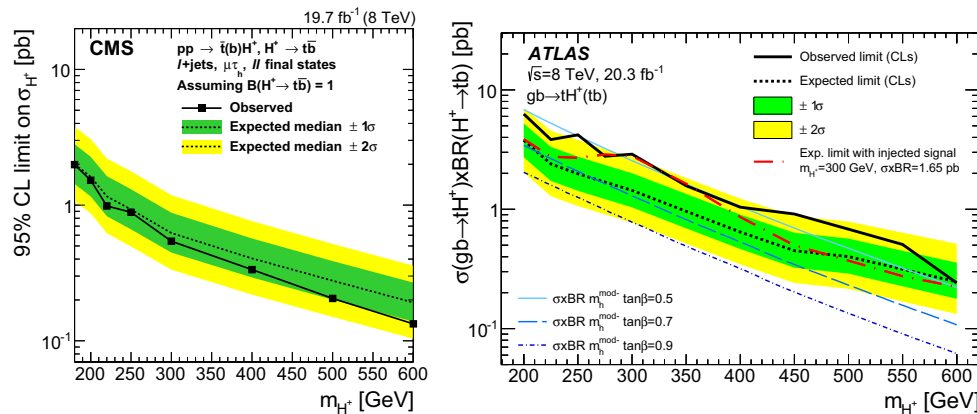


**Fig. 23** *Left* CMS upper limits on $\sigma(pp \to t(b)H^+)$ for the combination of the $\mu\tau_h$, $\ell +$ jets, and $\ell\ell'$ final states assuming $\mathrm{BR}(H^+ \to t\bar{b}) = 100\%$. (Reprinted with kind permission from JHEP and the authors, Fig. 10 of [216]). *Right* ATLAS upper limits for the production of $H^+ \to t\bar{b}$ in association with a top quark. The *red dash-dotted line* shows the expected limit obtained for a simulated signal injected at $M_{H^\pm} = 300$ GeV. (Reprinted with kind permission from JHEP and the authors, Fig. 6 of [219])

**Fig. 24** ATLAS limits on the *s*-channel production *cross section* times branching fraction for $H^+ \to t\bar{b}$ as a function of the charged Higgs-boson mass, for particular final states, using the narrow-width approximation. (Reprinted with kind permission from JHEP and the authors, Fig. 10 of [219])
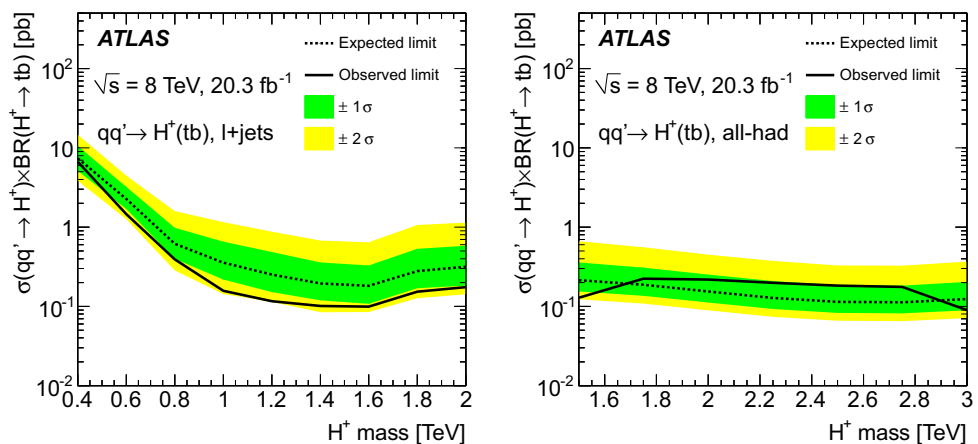


### 7.2.5 LHC constraints from the neutral Higgs sector

After the discovery in 2012 of the SM-like Higgs particle with a mass of 125 GeV, measurements of its properties lead to serious constraints on the parameters space of the 2HDM, among others on the mass of the $H^+$.

Constraints on the gauge coupling of the lightest neutral 2HDM Higgs boson were recently obtained by ATLAS [222]

**Fig. 25** ATLAS regions of the $[\cos(\beta - \alpha), \tan\beta]$ plane for the 2HDM Model I (*left*) and Model II (*right*) excluded by fits to the measured rates of Higgs-boson production and decays. (Reprinted with kind permission from JHEP and the authors, Fig. 5 of [222])
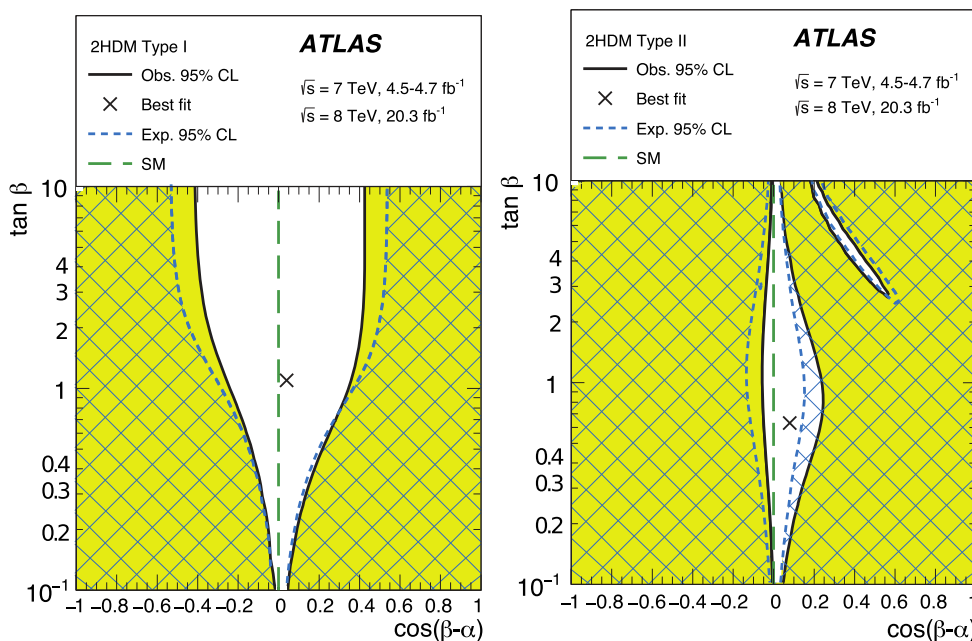


for four Yukawa models. The results support the SM-like scenario for $h$ with $\sin(\beta - \alpha) \approx 1$, the allowed (95% CL) small value of $\cos(\beta - \alpha)$, e.g. for Model II is up to 0.2 for $\tan\beta = 1$ while it extends up to $\pm 0.4$ for large $\tan\beta$ in Model I; see Fig. 25. There are also "wrong-sign" regions allowed for Yukawa couplings for larger values of $\cos(\beta - \alpha)$ for Model II, as mentioned in Sect. 4.

Two further aspects of the recent model-independent neutral-Higgs studies at the LHC [223,224] are important:

(i)  The production and subsequent decay of a neutral Higgs $H_1$ to $\gamma\gamma$, at $M = 125$ GeV should be close to the SM result. Assuming the dominant production to be via gluon fusion (and adopting the narrow-width approximation), this can be approximated as a constraint on

$$R_{\gamma\gamma} = \frac{\Gamma(H_1 \to gg)\mathrm{BR}(H_1 \to \gamma\gamma)}{\Gamma(H_{\mathrm{SM}} \to gg)\mathrm{BR}(H_{\mathrm{SM}} \to \gamma\gamma)}. \qquad (7.6)$$

For Model II channels discussed in Sect. 8.3 [62,121], a generous range $0.5 \le R_{\gamma\gamma} \le 2$ was adopted, whereas recent ATLAS and CMS results ($\pm 2\sigma$ regions) are $0.63 \le R_{\gamma\gamma} \le 1.71$ [225] and $0.64 \le R_{\gamma\gamma} \le 1.6$ [3], respectively. Note that this quantity is sensitive to the $H^+$, since its loop contribution proportional to the $H_1 H^+ H^-$ coupling can have a constructive or destructive interference with the SM contribution. The non-decoupling property of the $H^+$ contribution to the $H_1 \to \gamma\gamma$ effective coupling may lead to sensitivity to even a very heavy $H^+$ boson.

(ii)  The production and subsequent decay, dominantly via $ZZ$ and $WW$ are constrained in the mass ranges of heavier neutral Higgs bosons $H_2$ and $H_3$ from 130 to

500 GeV. We consider the quantity

$$R_{ZZ} = \frac{\Gamma(H_j \to gg)\mathrm{BR}(H_j \to ZZ)}{\Gamma(H_{\mathrm{SM}} \to gg)\mathrm{BR}(H_{\mathrm{SM}} \to ZZ)}, \qquad (7.7)$$

for $j = 2, 3$, and require it to be below the stronger 95% CL obtained by ATLAS or CMS in the scans described in Sect. 8.3.

## 8 Further search for $H^+$ at the LHC

Here, a discussion of possible search strategies for charged scalars at the LHC is presented. The stakes of a possible discovery from an extended scalar sector are very high, these searches should be pursued in all conceivable channels. Some propositions are described below, separately for low and high masses of the $H^+$ boson.

As discussed in previous sections, a light charged Higgs boson is only viable in Models I and X. In the more familiar Model II (and also Y), the $B \to X_s\gamma$ constraint enforces $M_{H^\pm} \gtrsim 480$ GeV or even higher for all values of $\tan\beta$ [13].

### 8.1 Channels for $M_{H^\pm} \lesssim m_t$

For low $M_{H^\pm}$ mass, the proposed searches can be divided into two categories, based on single $H^+$ production or $H^+H^-$ pair production. For all channels presented here, $\tau\nu$ decays of charged Higgs bosons are the recommended ones.

**Table 3** Proposed channels, denoted by $\sqrt{}$, for Models I and X at 30 fb$^{-1}$. The case denoted by ($\sqrt{}$) requires higher luminosity

| $M_{H^\pm}$ | 100 GeV | | 150 GeV | |
|---|---|---|---|---|
| $\tan\beta$ | 3 | 10 | 3 | 10 |
| $H^+W^-b\bar{b}$ (6.3b) | $\sqrt{}$ | $\sqrt{}$ | $\sqrt{}$ | |
| $H^+bq$ (6.4) | $\sqrt{}$ | ($\sqrt{}$) | $\sqrt{}$ | |

**Table 4** Proposed channels, denoted by $\sqrt{}$, for Models I and X, requiring resonant production, at 30 fb$^{-1}$. The cases denoted by ($\sqrt{}$) would need higher luminosity

| $M_{H^\pm}$ | 100 GeV | | | 150 GeV | | |
|---|---|---|---|---|---|---|
| $\tan\beta$ | 3 | 10 | 30 | 3 | 10 | 30 |
| $H^+W^-$ (6.1) | $\sqrt{}$ | ($\sqrt{}$) | | $\sqrt{}$ | ($\sqrt{}$) | |
| $H^+H^-$ (6.10a) | $\sqrt{}$ | $\sqrt{}$ | $\sqrt{}$ | $\sqrt{}$ | $\sqrt{}$ | $\sqrt{}$ |
| $H^+H^-q'Q'$ (6.10b) | $\sqrt{}$ | $\sqrt{}$ | $\sqrt{}$ | $\sqrt{}$ | $\sqrt{}$ | $\sqrt{}$ |

### 8.1.1 Single $H^+$ production

In Ref. [226] processes with a single $H^+$ were studied for Models I and X. Here, the production mechanism depends on the $H^+b\bar{t}$ Yukawa coupling, proportional to $1/\tan\beta$, thus falling off sharply at high $\tan\beta$. Concentrating on processes without neutral-Higgs-boson intermediate states[13] [Eqs. (6.4)–(6.6)], it was found that for 30 fb$^{-1}$ of integrated luminosity the reach at the 95% CL allows exploring low values of $\tan\beta$, up to about 10. At higher values of $\tan\beta$, the Model I branching ratio for $t \to H^+b$ becomes too small (see Fig. 5) for the search to be efficient. In Table 3 we present promising parameters for two proposed channels from this analysis.

### 8.1.2 $H^+H^-$ pair production

Charged Higgs-boson pair production, see Eq. (6.10) and Figs. 13 and 14, can be sensitive also to higher values of $\tan\beta$ [226]. This will require resonant production via $H_j$ decaying to $H^+H^-$, and assuming an enhancement of the coupling between charged and neutral Higgs bosons. In Table 4 we present channels which would be viable in the case of resonant intermediate $H_j$ states, as represented by the mechanism of Fig. 13a (i).

### 8.2 Channels for $m_t < M_{H^\pm} < 480$ GeV

The intermediate-mass region requires a dedicated discussion, since only Models I and X are allowed. However, in contrast to the $M_{H^\pm} < m_t$-region, the $H^+ \to t\bar{b}$ channel

---

[13] This process, involving neutral scalars $H_j$, depends on the Yukawa model and needs a dedicated analysis [54,227].

is now open. Also the channel $H^+ \to W^+h$ is open in the higher mass range. These channels may thus compete with the $\tau\nu$ channel discussed for the low-mass case. Whereas the cross section becomes very small at high $\tan\beta$, where the $\tau\nu$ channel is interesting (see Fig. 15, left panel), these other channels could be interesting at lower values of $\tan\beta$.

### 8.3 Channels for 480 GeV $< M_{H^\pm}$

For high masses, all four Yukawa models are permitted, and there are three classes of decay channels, $H^+ \to H_1W^+$ (or $AW^+$, $HW^+$, $hW^+$), $H^+ \to \tau^+\nu$ and $H^+ \to t\bar{b}$. We shall here present studies of the first two, which only compete with a moderate QCD background. Within the 2HDM II, like in the MSSM [228,229], the decay channel (5.3), $H^+ \to H_1W^+$, can be used, with $H_1 \to b\bar{b}$. The $t\bar{b}$ channel competes with an enormous QCD background, but recent progress in $t$ and $b$ tagging have yielded the first results, as reported in Sect. 7.2.3.

### 8.3.1 The channel $H^+ \to W^+H_j \to W^+b\bar{b}$

A study [230] of the process $pp \to H^+\bar{t}$ in Model II, where the charged Higgs boson decays to a $W$ and the observed Higgs boson at 125 GeV, which in turn decays to $b\bar{b}$, for charged-Higgs mass up to about 500 GeV, concludes that an integrated luminosity of the order of 3000 fb$^{-1}$ is required for a viable signal.

This search channel has recently been re-examined for Model II, for high charged-Higgs mass and neutral-Higgs masses all low [231]. The discovered 125 GeV Higgs boson is taken to be $H$, the heavier CP-even one. Thus, the charged one could decay to $WH$, $WA$ and $Wh$. The dominant production mode at high charged-Higgs mass is from the channel (6.2), $\bar{b}g \to H^+\bar{t} \to H^+\bar{b}W^-$. There will thus be at least three $b$ quarks in the final state, two of which will typically come from one of the neutral Higgs bosons:

$$pp(\bar{b}g) \to H^+\bar{t}X \to H^+\bar{b}W^-X \to b\bar{b}\bar{b}W^+W^-X \to b\bar{b}\bar{b}\ell\nu jjX. \tag{8.1}$$

Interesting parameter regions are identified for $\tan\beta = \mathcal{O}(1)$, and $\sin(\beta-\alpha)$ close to 0 (the discovered Higgs boson is the $H$), where a signal can be extracted over the background. The fact that the $H^+$ is heavy, means that the $W^+$ from its decay will be highly boosted. This fact is exploited to isolate the signal. Since the interesting region has $\tan\beta = \mathcal{O}(1)$, this channel remains relevant also for other Yukawa types.

Relaxing CP conservation, this option has been explored in [121]. Imposing the theoretical and experimental constraints discussed in Sects. 3 and 7, one finds a surviving parameter space that basically falls into two regions: (i) low $\tan\beta$, with non-negligible CP violation and a considerable

**Table 5** Suggested points selected from the allowed parameter space [121]. Note that $M_3$ is not an independent parameter. Furthermore, $\mu = 200$ GeV

| $\alpha_1/\pi$ | $\alpha_2/\pi$ | $\alpha_3/\pi$ | $\tan \beta$ | $M_2$ (GeV) | $M_3$ (GeV) |
|---|---|---|---|---|---|
| 0.35 | −0.056 | 0.43 | 1 | 400 | 446 |
| 0.33 | −0.21 | 0.23 | 1 | 450 | 524 |

branching ratio $H^+ \to H_1 W^+$ (see Sect. 5.4), and (ii) high $\tan \beta$, with little CP violation and only a modest decay rate $H^+ \to H_1 W^+$.

For the region (i), the channel

$$pp \to H^+ W^- X \to H_1 W^+ W^- X \to b\bar{b}\ell\nu jj X \qquad (8.2)$$

has been studied (see also Ref. [62]). A priori, there is a considerable $t\bar{t}$ background. However, imposing a series of kinematical cuts, it is found that this background can be reduced to a manageable level, yielding sensitivities of the order of 2–5 for a number of events of the order of 10–20, with an integrated luminosity of 100 fb$^{-1}$ at 14 TeV. A more sophisticated experimental analysis could presumably improve on this. The more promising parameter points are presented in Table 5. No point was found at higher values of $\tan \beta$ ($\gtrsim 2$), within the now allowed range of $M_{H^\pm}$.

While the above analysis focused on the bosonic production mode, where resonant production via $H_2$ or $H_3$ is possible, a study of the fermionic mode,

$$pp(gg) \to H^+ \bar{t} b X \to t \bar{t} b \bar{b} X, \qquad (8.3)$$

has been performed for the maximally symmetric 2HDM, which is based on the SO(5) group, and has natural SM alignment [232]. In this analysis, the "stransverse" mass, $M_{T2}$ [233], is exploited, and it is found that by reconstructing at least one top quark, a signal can be isolated above the SM background.

### 8.3.2 The channel $H^+ \to \tau^+ \nu$

The $H^+ \to \tau^+ \nu$ channel is traditionally believed to have little background. However, a recent study of Model II finds [62] that this channel can only be efficiently searched for at some future facility at a higher energy. This is due to a combination of many effects. At high mass ($M_{H^\pm} \gtrsim 480$ GeV) the production rate goes down, whereas a variety of multi-jet processes also give events with an isolated $\tau$ and missing momentum.

### 8.3.3 The channel $H^+ \to t\bar{b}$

As discussed in Sect. 5, except for particular parameter regions allowing the $H^+ \to W^+ H_j$ modes, at high values

of $M_{H^\pm}$ the $t\bar{b}$ channel is the dominant one. This channel has long been ignored because of the enormous QCD background, but methods are being developed to suppress this, as exemplified in Ref. [219].

### 8.3.4 Exploiting top polarization

At high masses the $bg \to H^- t$ production mechanism is dominant. If the $H^+$ decays fully hadronically and its mass is known, then semileptonic decays of the top quark can be analyzed in terms of its polarization. Such studies can yield information on $\tan \beta$, since this parameter determines the chirality of the $H^+ tb$ coupling [234–238].

## 8.4 Other scenarios

Various scenarios for additional Higgs bosons have been discussed in the literature. These typically assume CP conservation. Several scenarios [239,240] and channels have recently been presented, mostly focussing on the neutral sector, in particular the phenomenology of the heavier CP-even state, $H$. In the "Scenario D (Short cascade)" of Ref. [239], it is pointed out that if $H$ is sufficiently heavy, it may decay as $H \to H^+ W^-$, or even as $H \to H^+ H^-$. A version of the former is discussed above, in Sect. 8.3, for Model II. In "Scenario E (Long cascade)", it is pointed out that for heavy $H^+$, one may have the chain $H^+ \to A W^+ \to H Z W^+$ or $H^+ \to H W^+$, whereas a heavy $A$ may allow $A \to H^+ W^- \to H W^+ W^-$. The modes $H^+ \to H W^+$ and $H^+ \to A W^+$ have also recently been discussed in Refs. [241,242].

The class of $bW$ production mechanisms $qb \to q' H^+ b$ depicted in Fig. 10 has been explored in Ref. [243], where it is pointed out that in the alignment limit, with neutral Higgs masses close, $M_A \simeq M_H$, there is a strong cancellation among different diagrams. Thus, if $M_A$ should be light, this mechanism would be numerically important. It is also suggested that the $p_T$-distribution of the $b$-jet may be used for diagnostics of the production mechanism.

## 9 Models with several charged scalars

### 9.1 Multi-Higgs-doublet models

Multi-Higgs Doublet Models (MHDM) are models with $n$ scalar SU(2) doublets, where $n \geq 3$ [191]. The $n = 1$ case corresponds to the Standard Model, the $n = 2$ case corresponds to the 2HDM, the main topic of this paper. New phenomena will appear for $n \geq 3$, for which we below often use the abbreviation MHDM. The MHDM has the virtue of predicting $\rho = 1$ at tree level, as does the 2HDM. In the MHDM there are $n - 1$ charged-scalar pairs, $H_i^+$. We shall
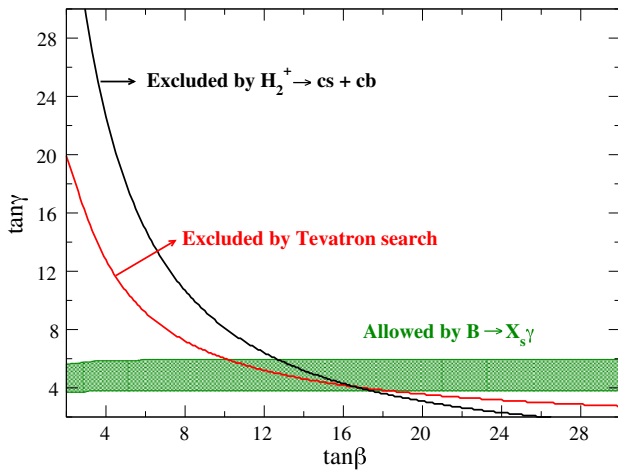
**Fig. 26** *Left* Allowed parameter space for the 3HDM (Model Y) with $M_{H_1^\pm} = 83$ GeV, $M_{H_2^\pm} = 160$ GeV and the mixing angle $\theta_C = -\pi/4$. Only the *green shaded region* is allowed by the $B \to X_s \gamma$ constraint.
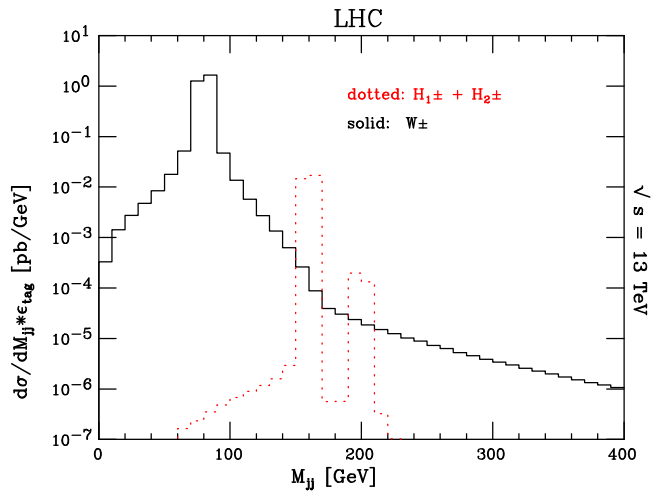
*Right* Di-jet invariant mass distributions for signal (*red*) and background (*black*) for a particular benchmark point (3HDM, Model Y) at the 13 TeV LHC

discuss only the phenomenology of the lightest $H^+$ ($\equiv H_1^+$), assuming that the other $H^+$ are heavier.

The Yukawa interaction of an $H_i^+$, $i = 1, \dots, n-1$ is described by the Lagrangian:

$$\mathcal{L}_{\mathrm{ch}} = \frac{g}{\sqrt{2}\, m_W}$$
$$\times \left\{ \left[ \bar{u} \left( m_d P_R \mathcal{F}_i^D + m_u P_L \mathcal{F}_i^U \right) d + \bar{\nu} m_\ell P_R \mathcal{F}_i^L \ell \right] H_i^+ + \text{h.c.} \right\}. \tag{9.1}$$

It applies to the 2HDM ($n = 2$); then the $\mathcal{F}$s given in Table 6 of Appendix A coincide with the $\mathcal{F}_1$ in the above equation. In general, the $\mathcal{F}_i^D$, $\mathcal{F}_i^U$ and $\mathcal{F}_i^L$ are complex numbers, which are defined in terms of an $n \times n$ matrix $U$, diagonalizing the mass matrix of the charged scalars.[14]

It is evident that the branching ratios of the charged Higgs bosons, $H_i^+$ depend on the parameters $\mathcal{F}_i^D$, $\mathcal{F}_i^U$ and $\mathcal{F}_i^L$. In the case of the 2HDM this shrinks to a single parameter, $\tan \beta$, which determines these three couplings. This implies that certain combinations are constrained, for example, in Model II we have, for each $i$, $|\mathcal{F}_i^D \mathcal{F}_i^U| = 1$.

As in the 2HDM (Models II and Y), an important constraint on the mass and couplings of $H^+$ in the MHDM is provided by the decay $B \to X_s \gamma$. However, here, even a light $H^+$ (i.e., $M_{H^\pm} \lesssim m_t$) is still a possibility, because of a cancellation between the loop contributions from the different scalars. Recently, $2\sigma$ intervals in the $\mathcal{F}_1^D - \mathcal{F}_1^U$ parameter space for $M_{H^\pm} = 100$ GeV were derived from $B \to X_s \gamma$ [49,244,245], assuming $|\mathcal{F}_1^U| < 1$, in order to comply with constraints from $Z \to b\bar{b}$.

---

[14] For details, see Ref. [191], where $\mathcal{F}_i^D$, $\mathcal{F}_i^U$ and $\mathcal{F}_i^L$ are denoted $X_i$, $Y_i$ and $Z_i$, respectively.

The fully active 3HDMs with two softly broken discrete $Z_2$ symmetries have two pairs of charged Higgs bosons, $H_1^\pm$ and $H_2^\pm$, studied in [246]. Depending on the $Z_2$ parity assignment, there are different Yukawa interactions. In each of these, the phenomenology of the charged Higgs bosons is in the CP-conserving case described by five parameters: the masses of the charged Higgs bosons, two ratios of the Higgs vev's $\tan \beta$ and $\tan \gamma$ and a mixing angle $\theta_C$ between $H_1^+$ and $H_2^+$. The BR($B \to X_s \gamma$) is determined by $W^+$, $H_1^+$ and $H_2^+$ loop contributions. The scenario with masses of $\mathcal{O}(100)$ GeV for the charged Higgs bosons is allowed. Therefore, the search for a light charged Higgs boson, which in some Yukawa models dominantly decays into $c\bar{b}$, may allow one to distinguish 3HDMs from 2HDMs. Some results are presented in Fig. 26 for the 3HDM Model Y.

Experimental constraints on $t \to H^+ b$ followed by $H^+ \to \tau^+ \nu$ and $H^+ \to c\bar{s} + c\bar{b}$ are relevant here. Scenarios with both $M_{H_1^\pm}$, $M_{H_2^\pm} \lesssim m_t$ are highly constrained from $B \to X_s \gamma$ and the LHC direct searches. The particular case $M_{H_1^\pm} \simeq m_W$ with 90 GeV $< M_{H_2^\pm} < m_t$ is allowed (also by the Tevatron and LEP2). The region of 80 GeV $< M_{H_1^\pm} < 90$ GeV is not constrained by current LHC searches for $t \to H^+ b$ followed by the dominant decay $H^+ \to c\bar{s}/c\bar{b}$, and this parameter space is only weakly constrained from LEP2 and Tevatron searches; see Fig. 26 (left). Any future signal in this region could readily be accommodated by $H_1^\pm$ from a 3HDM.

A Monte Carlo simulation of the $H_{1,2}^+$ signals and $W^+$ background via the processes $gg, q\bar{q} \to t\bar{b} H_{1,2}^-$ and $gg, q\bar{q} \to t\bar{b} W^-$, respectively, followed by the corresponding di-jet decays is shown in Fig. 26 (right). The charged Higgs-boson signals should be accessible at the LHC, pro-

**Fig. 27** *Left* Contours of BR($H^+ \to cb$) in the $|\mathcal{F}_1^D|-|\mathcal{F}_1^U|$-plane with $|\mathcal{F}_1^L| = 0.1$. The $B \to X_s\gamma$ constraint removes the region above the red or blue hyperbolas; see the text. Note that the two scales on the axes are very different. *Right* Contours of BR($t \to H^+b$) × BR($H^+ \to cb$)
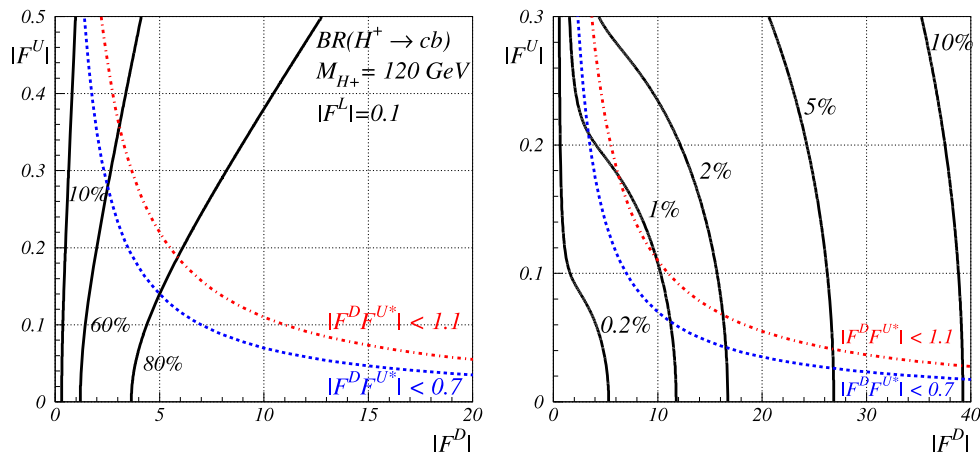


vided that $b$-tagging is enforced so as to single out the $c\bar{b}$ component above the $c\bar{s}$ one (see the following subsection). Therefore, these (multiple) charged Higgs-boson signatures can be used not only to distinguish between 2HDMs and 3HDMs but also to identify the particular Yukawa model realizing the latter. Some benchmark points are provided in [246].

### 9.2 Enhanced $H^+ \to c\bar{b}$ branching ratio

In the 2HDM, the magnitude of BR($H^+ \to c\bar{b}$) is always less than a few percent, with the exception of Model Y (see Fig. 1), since the decay rate is suppressed by the small CKM element $V_{cb}$ ($\ll V_{cs}$).

A distinctive signal of $H^+$ from a 3HDM for $M_{H^+} \lesssim m_t$ could be a sizable branching ratio for $H^+ \to c\bar{b}$ [15,191, 247]. The scenario with $|\mathcal{F}_1^D| \gg |\mathcal{F}_1^U|, |\mathcal{F}_1^L|$ corresponds to a "leptophobic" $H^+$ with[15] BR($H^+ \to c\bar{s}$) + BR($H^+ \to c\bar{b}$) $\sim$100%.

In this limit, the ratio of BR($H^+ \to c\bar{b}$) and BR($H^+ \to c\bar{s}$) can be expressed as follows:

$$\frac{\text{BR}(H^+ \to c\bar{b})}{\text{BR}(H^+ \to c\bar{s})} \equiv R_{bs} \sim \frac{|V_{cb}|^2}{|V_{cs}|^2} \frac{m_b^2}{m_s^2}. \tag{9.2}$$

In Ref. [248] the magnitude of BR($H^+ \to c\bar{b}$) as a function of the couplings $\mathcal{F}_1^U$, $\mathcal{F}_1^D$ and $\mathcal{F}_1^L$ was studied, updating the numerical study of [15]. As an example, in Fig. 27 (left), BR($H^+ \to c\bar{b}$) in a 3HDM is displayed in the $|\mathcal{F}_1^D|-|\mathcal{F}_1^U|$-plane for $M_{H^\pm} = 120$ GeV, with $|\mathcal{F}_1^L| = 0.1$. The maximum value is BR($H^+ \to c\bar{b}$) $\sim$81%. The bound from $B \to X_s\gamma$ is also shown, which is $|\mathcal{F}_1^D\mathcal{F}_1^U| < 1.1$ (0.7) for $\mathcal{F}_1^D\mathcal{F}_1^{U*}$ being real and negative (positive).

Increased sensitivity can be achieved by requiring also a $b$-tag on the jets from the decay of $H^+$. In Fig. 27 (right) for $M_{H^\pm} = 120$ GeV we show contours of BR($t \to H^+b$) ×

BR($H^+ \to c\bar{b}$), starting from 0.2%, accessible at the LHC. In this case, a large part of the region of $|\mathcal{F}_1^D| < 5$ could be probed, even for $|\mathcal{F}_1^U| < 0.2$.

In summary, a distinctive signal of $H^+$ from a 3HDM for $M_{H^+} \lesssim m_t$ could be a sizable branching ratio for $H^+ \to c\bar{b}$. A dedicated search for $t \to H^+b$ and $H^+ \to c\bar{b}$, in which the additional $b$-jet originating from $H^+$ is tagged, would be a well-motivated and (possibly) straightforward extension of the ongoing searches with the decay $H^+ \to c\bar{s}$.

## 10 Models with charged scalars and DM candidates

It is possible that the issues of dark matter (DM) and mass generation are actually related.[16] Such models must of course contain a Standard-Model-like neutral Higgs particle, with mass at $M_h = 125$ GeV. Additionally, there appear charged Higgs particles and other charged (as well as neutral) scalars. In these models, the DM relic density provides a constraint on the charged scalars.

In order to have a stable DM candidate some $Z_2$ symmetry is typically introduced, under which an SU(2) singlet or doublet involving the DM particle, is odd. The $Z_2$-odd scalars are often called dark scalars. Among them, the lightest neutral one is a DM candidate. Below, we will denote the charged ones $S^+$, and the neutral ones $A$ and $S$, with $S$ being the lightest. In some models, there may be several scalars, then referred to as $S_i^+$ and $S_i$.

Typically, the charged scalars of these models have some features in common with the charged Higgs of Model I (and X). They do not couple to the $b$ and $s$ quarks (in fact, they do not couple to *any* fermion), and thus are not affected by the $B \to X_s\gamma$ constraint. Hence, they can be rather light. LEP searches for charginos can be used to establish a lower mass bound of about 70 GeV [250] for such charged scalars.

---

[15] A similar situation arises in the 2HDM (Y), for $\tan\beta \gg 3$.

[16] The SM Higgs-boson mass term, $\sim \Phi^\dagger\Phi$, may allow for a connection (Higgs portal) to a hypothetical hidden sector [249].

The first model which allows this relationship between the Higgs and DM sectors was introduced many years ago [29], and will here be referred to as the "Inert Doublet Model", or IDM [251–253].[17] Here, one SU(2) doublet ($\Phi_1$) plays the same role as the SM scalar doublet, the other one with zero vacuum expectation value does not couple to fermions. An extension of this model with an extra doublet [254–257] or a singlet [258] allows also for CP violation. This improves the prospects for describing baryogenesis [19].

Alternatively, a $Z_2$-odd scalar SU(2) singlet $\mathcal{S}$ [259–262] mixed with a $Z_2$-odd scalar SU(2) doublet $\Phi_2$ may provide a framework for dark matter.[18] It was shown in Refs. [263,264] that the high-energy theory leading to electroweak-scale scalar DM models can be a non-SUSY SO(10) Grand Unified Theory (GUT) [265]. Indeed, the discrete $Z_2$ symmetry, which makes DM stable, could be an unbroken discrete remnant of some underlying U(1) gauge subgroup [266–268]. Unlike in the IDM, in the GUT-induced scalar DM scenario the lightest dark scalar is predicted by RGEs to be dominantly singlet.

A corresponding charged dark scalar $S^+$ can be searched for in the decays

$$S^+ \rightarrow S_i f \bar{f}',\tag{10.1}$$

mediated by a virtual or real $W^\pm$, where $S_i$ is a neutral dark scalar, and $f$ and $f'$ denote SM fermions.

The production at the LHC of $S^+ S^-$ pairs, $pp \rightarrow S^+ S^-$, and of $S^+$ together with neutral dark scalars $pp \rightarrow S^+ S_i$ was investigated [107,269–271]. Because of relic density and electroweak precision measurement constraints, $S^+$ and $S$ tend to be close in mass, $M_{S^\pm} - M_S \ll m_W$. In such regions of parameter space, and in the limit of massless fermions, the $S^+$ width is [272]

$$\Gamma(S^+ \rightarrow S f \bar{f}') = \frac{G_F^2}{30\pi^3}(M_{S^\pm} - M_S)^5,\tag{10.2}$$

so the $S^+$ will be long-lived and travel a macroscopic distance.

## 10.1 The inert doublet model, IDM

The Inert Doublet Model can be defined in terms of the potential

$$V_{\text{IDM}} = -\frac{1}{2}\left\{m_{11}^2 \Phi_1^\dagger \Phi_1 + m_{22}^2 \Phi_2^\dagger \Phi_2\right\} + \frac{\lambda_1}{2}(\Phi_1^\dagger \Phi_1)^2$$
$$+ \frac{\lambda_2}{2}(\Phi_2^\dagger \Phi_2)^2 + \lambda_3(\Phi_1^\dagger \Phi_1)(\Phi_2^\dagger \Phi_2)$$
$$+ \lambda_4(\Phi_1^\dagger \Phi_2)(\Phi_2^\dagger \Phi_1) + \frac{1}{2}\left[\lambda_5(\Phi_1^\dagger \Phi_2)^2 + \text{h.c.}\right].\tag{10.3}$$

This is the same potential as in Eq. (2.1), but without the $Z_2$-breaking term proportional to $m_{12}^2$, and hence with $\lambda_5$ real; see Eq. (2.10).

The charged-scalar mass coming from Eq. (10.3) is given by

$$M_{S^\pm}^2 = -\frac{m_{22}^2}{2} + \frac{\lambda_3 v^2}{2}.\tag{10.4}$$

The parameter $\lambda_3$ also governs the coupling of the $S^+$ to the Higgs particle $h$.

Perturbative unitarity constraints on other lambdas, together with precision data on the electroweak parameters $S$ and $T$, limit masses of the dark scalars to less than 600 GeV for $S$ and less than 700 GeV for $A$ and $S^+$, for $|m_{22}^2|$ below $10^4$ GeV$^2$. Much heavier dark particles are allowed for large, negative values of $m_{22}^2$, e.g. $M_A$, $M_S$, $M_{S^\pm}$ can take values up to 1 TeV for $m_{22}^2 = -(1 \text{ TeV})^2$.

Measurements of $R_{\gamma\gamma}$ strongly constrain masses and couplings of dark particles, the closer to 1 is this ratio, the higher the masses of dark particles, including $S^+$, are allowed. Enhancement of this ratio above 1 would only be possible if there were no open invisible channels ($2M_S > M_h$). For example, for $R_{\gamma\gamma} > 1.3$ the range of $M_{S^\pm}$ would have to be below $\sim$135 GeV.

If the model is required to saturate the relic DM abundance, then $M_{S^\pm}$ has to be below approximately 300 GeV, or else above $\sim$500 GeV. In the latter case, its mass is very close to that of the DM particle. On the other hand, if the model is not required to saturate the DM relic abundance, then only not to produce too much DM, then the charged-scalar mass is less constrained [273].

Analyses based on an extensive set of theoretical and experimental constraints on this model have recently been performed, both at tree level [273,274] and at loop level [26]. Collider as well as astroparticle data limits were included, the latter in the form of dark matter relic density as well as direct detection data. A minimal scale of 45 GeV for the dark scalar mass, and a stringent mass hierarchy $M_{S^\pm} > M_A$ are found [273]. Parameter points and planes for dark scalar pair production $S^+ S^-$ for the current LHC run are proposed, with $S^+$ masses in the range 120–450 GeV [273]. It is found that the decay $S^+ \rightarrow W^+ S$ dominates, and $M_{S^\pm} - M_S > 100$ MeV. A heavier $S^+$ benchmark ($M_{S^\pm} > 900$ GeV) is also proposed [26].

## 10.2 The CP-violating inert doublet model, IDM2

If the above model is extended with an extra doublet, one can allow for CP violation, like in the 2HDM [254,255]. There are then a total of three doublets, one of which is inert in the sense that it has no vacuum expectation value, and hence no coupling to fermions. This kind of model will have two charged scalars, one ($H^+$) with fermionic couplings and phenomenology similar to that of the 2HDM (but the constraints on the parameter space will be different, due to the extra degrees of freedom), and one ($S^+$) with a phenomenology similar to that of the IDM.

The charged scalar $S^+$ could be light, down to about 70 GeV. Its phenomenology has been addressed in [272]. The allowed ranges for the DM particle are similar to those found for the IDM, a low-to-intermediate-mass region up to about 120 GeV, and a high-mass region above about 500 GeV.

The decay modes of the additional charged scalar are the same as in the IDM, it decays either to a $W$ and a DM particle, or to a $Z$ and the neutral partner of the DM particle [272]. In the low-to-intermediate $S^+$ mass region, the $W$ and $Z$ could be virtual.

## 10.3 One or two inert doublets within 3HDM

In the context of 3HDMs, models with one or two inert doublets were considered, involving new charged Higgs and/or charged inert scalars. (The IDM2 model discussed above, is one such case, allowing for CP violation.) The richer inert particle spectrum for the case with two inert doublets enables a variety of co-annihilation channels of the DM candidate, including those with two different pairs of charged inert bosons [256,257]. This allows one to relieve the tension in current experimental constraints from Planck, LUX and the LHC. As a consequence, new DM mass regions open up, both at the light ($M_S \lesssim 50$ GeV) and heavy (360 GeV $\lesssim M_S \lesssim 500$ GeV) end of the spectrum, which are precluded to the IDM and are in turn testable at the LHC. Concerning LHC phenomenology of visible channels, a smoking gun signature of the model with two inert doublets is a new decay channel of the next-to-lightest inert scalar into the scalar DM candidate involving (off-shell) photon(s) plus missing energy [275], which is enabled by $S_i^+ W^-$ loops. The hallmark signal for the model with one inert doublet would be significantly increased $H^+ \rightarrow W^+ Z$ and $W^+ \gamma$ decay rates (in which a key role is played by loops involving the $S^+$ state) with respect to the IDM [276]. This new phenomenology is compliant with the most up-to-date constraints on the respective parameter spaces, both experimental and theoretical [277].

## 10.4 SO(10) and the GUT-induced scalar DM scenario

The GUT-induced scalar DM scenario with minimal particle content includes a Higgs boson in a **10** and the DM in a **16** representation of SO(10). One identifies here the $Z_2$ symmetry as the matter parity [263,264], defined as

$$P_M = (-1)^{3(B-L)}. \qquad (10.5)$$

Since the matter parity $P_M$ is directly related to the breaking of $B - L$, the dark sector actually consists of scalar partners of the SM fermions which carry the same gauge quantum numbers as the MSSM squarks and sleptons. In this scenario the origin and stability of DM, the non-vanishing neutrino masses via the seesaw mechanism [278–282] and the baryon asymmetry of the Universe via leptogenesis [283] all spring from the same source – the breaking of the SO(10) gauge symmetry.

The IDM represents just one particular corner of parameter space of the general $P_M$-odd scalar DM scenario in which the DM is predominantly doublet. A theoretically better motivated particle spectrum can be obtained by renormalization group (RG) evolution of the model parameters from the GUT scale to $m_Z$ [264], in a direct analogy with the way the particle spectrum is obtained in the constrained minimal supersymmetric standard model (CMSSM).[19] In the GUT-induced scalar DM model, the EWSB may occur due to the existence of dark scalar couplings to the Higgs boson. Moreover, such couplings can lower the stability bound and accommodate also a Higgs mass around 125 GeV [287].

Below the GUT scale $M_G$ and above the EWSB scale the model is described by the scalar potential for the doublets and the singlet:

$$V = V_{IDM} + \text{terms bilinear and quartic in } \mathcal{S}, \qquad (10.6)$$

invariant under

$$(\Phi_1, \Phi_2, \mathcal{S}) \leftrightarrow (\Phi_1, -\Phi_2, -\mathcal{S}), \qquad (10.7)$$

and with $V_{IDM}$ defined by Eq. (10.3). The charged-scalar mass of this model is determined by $V_{IDM}$ and given by Eq. (10.4).

The mass degeneracy of $S$ and the next-to-lightest neutral scalar, denoted $S_{NL}$, is a generic property of the scenario and follows from the underlying SO(10) gauge symmetry. It implies a long lifetime for $S_{NL}$, which provides a clear experimental signature of a displaced vertex in the decays $S_{NL} \rightarrow S\ell^+\ell^-$ at the LHC [288].

## 10.5 Dark charged-scalar phenomenology at the LHC

Compared to the $H^+$ of 2HDM models, dark $S^+$ production lacks some primary parton-level processes, since it has to be

---

[19] To obtain successful EWSB at low energies ($\sim m_Z$) the mass parameter $m_{11}^2$ in Eq. (10.3) can become positive either by the RG evolution [264] or via a Coleman–Weinberg-like [284] mechanism [285,286].
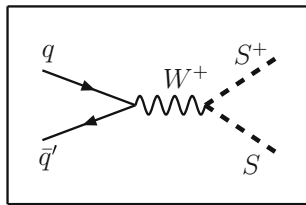
**Fig. 28** Feynman diagram for associated dark $S^+S$ production at the LHC

produced in association with a neutral dark-sector particle, as illustrated in Fig. 28, or else pair produced via $\gamma$, $Z$ or $H_j$ in the $s$-channel (see Fig. 13).

The early literature [107,252,269,270] on the IDM was mostly aimed at guiding the search for evidence on the model, via the production of the charged member, $S^+$, together with a neutral one. It focused on a DM mass of the order of 60–80 GeV, and a charged state $S^+$ with a mass of the order of 100–150 GeV. For these masses, the production cross sections are at 14 TeV of the order of 100–500 fb, and the two-[270] and three-lepton [107] channels were advocated. For an update on the allowed parameter space and proposed benchmark points; see Ref. [273].

While the $S^+S$ channel has the highest cross section, because of the larger phase space, its discovery is challenging. The $S^+$ would decay to an (invisible) $S$, plus a virtual $W^+$, giving a two-jet or a lepton-neutrino final state. The overall signal would thus be jets or an isolated charged lepton (from the $W$) plus missing transverse energy. If instead the heavier neutral state $A$ is produced together with the $S^+$, some of its decays (via a virtual $Z$) would lead to two-lepton and three-lepton final states [107,270]. Various cuts would permit the extraction of a signal against the $t\bar{t}$ and $WZ$ background. In the case of the very similar phenomenology of the IDM2, a study of $M_S = 75$ GeV with 100 fb$^{-1}$ of data concludes that the best $S^+$ search channel is in the hadronic decay of the $W$, leading to two merging jets plus missing transverse energy [272],

$$pp \rightarrow j + \text{MET}. \tag{10.8}$$

Recently, also the four-lepton modes for $S^+$ masses in the range 98–160 GeV have been studied [289], and one addressed constraints on the model from existing data on SUSY searches [290], considering two $S^+$ masses, 85 and 150 GeV. Another recent study of the $S^+S$ and $S^+A$ channels [291] concludes that the di-jet channel may offer the best prospects for discovery, but that a luminosity of 500 fb$^{-1}$ would be needed for an $S^+$ mass up to 150 GeV, whereas 1 and 2 ab$^{-1}$ for masses of 200 and 300 GeV.

In the above SO(10) scenario the mass difference $M_{S\pm} - M_S$ turns out to be less than $m_W$ and at the leading order

the allowed decays are only those given by Eq. (10.1) with a virtual $W$.

In some cases $S^+$ is so long-lived (decay length $\ell \gtrsim 1$ mm), due to an accidental mass degeneracy between $S^+$ and $S$ that it may decay outside the detector. Those experimental signatures are in principle background free and allow $S^+$ to be discovered at the LHC up to masses $M_{S\pm} \lesssim 300$ GeV.

To study charged-scalar pair production in the SO(10) scenario at the LHC, parameter points with distinctive phenomenologies are proposed [263,264,271,286–288]. For some parameter points, the $S^+$ decays inside the tracker of an LHC experiment. The experimental signature of those points is that the charged track of $S^+$ breaks into a charged lepton track and missing energy.

## 11 Summary and outlook

Since the summer of 2012 we are in the final stage of confirmation of the foundation of the SM. However, so far there is no clear clue for a further direction. Various SM-like models with extra Higgs scalars exist. A charged Higgs boson ($H^+$) would be the most striking signal of a Higgs sector with more than one Higgs doublet. Such a discovery at the LHC is a distinct possibility, with or without supersymmetry. However, a charged Higgs particle might be hard to find, even if it is abundantly produced.

For masses of the charged scalar below 500 GeV, a variety of 2HDM models remain viable, with $H^+$ decaying either to heavy flavors or to $\tau^+\nu$. Some of these have Model I-type Yukawa couplings, others arise in models that accommodate dark matter. Above 500 GeV, also Model II would be a possible interpretation. Here, the most "natural" decay modes would be to $t\bar{b}$ and $H_jW^+$, where $H_j$ could be any of the three neutral Higgs bosons.

If a signal were to be found, one of the first questions would be whether it is the charged Higgs of the MSSM or not. We note that the MSSM mass spectrum is very constrained; the heavier states should be close in mass. Secondly, the Yukawa couplings would at tree level be those of Model II. This means that the low-mass region would be severely constrained by $B \rightarrow X_s\gamma$, unless there is some cancellation of the $H^+$ contribution. A natural candidate would be a squark–chargino loop. But lower bounds on squark and chargino masses make this hard to arrange.

The charged Higgs boson can also be part of a higher representation. Additionally, in higher representations one could have doubly charged $H^{++}$, and also more "exotic" decay modes. For example, with a Higgs triplet, one could have [292] $H^+ \rightarrow W^+Z$ at tree level. Note however, a recent ATLAS analysis [293] excludes charged Higgs between 240 and 700 GeV if $H^+ \rightarrow W^+Z$ is the dominant decay mode. This could be the case for the Georgi–Machacek model [294].

This process is also possible in the 3HDM discussed in Sect. 9.1, but then only being generated at the one-loop level.

For the above-mentioned $H^+ \to H_j W^+$ decay modes, there are two competing effects. (i) Decay to the lightest state $H_1$ (or $h$) benefits from a non-negligible phase space, but vanishes in the alignment limit; see Eq. (2.13) and Fig. 6. (ii) Decays to the heavier ones, $H_2$ and $H_3$ (or $H$ and $A$), where couplings are not suppressed, suffer from a small phase space, since various constraint ($T$, in particular) force these masses to be close to $M_{H^\pm}$. In view of the convergence of measurements pointing to a CP-conserving Higgs sector, and alignment, the parameter space for the $H^+ \to H_j W^+$ decay modes is shrinking, and at high masses the $t\bar{b}$ mode may be the most promising one. However, the QCD background is very challenging, so improved analysis techniques could turn out to be very beneficial.

## Appendix A: Field decompositions

Breaking the electroweak symmetry spontaneously, we assume that the electrically neutral components of the Higgs doublets have non-zero expectation values, cf. Eq. (2.3). By assuming that they are real and positive, we define a basis in which

$$\langle \Phi_1 \rangle = \begin{pmatrix} 0 \\ \frac{v_1}{\sqrt{2}} \end{pmatrix}, \quad \langle \Phi_2 \rangle = \begin{pmatrix} 0 \\ \frac{v_2}{\sqrt{2}} \end{pmatrix} \tag{A.1}$$

with

$$\tan \beta = \frac{v_2}{v_1}. \tag{A.2}$$

Note that the introduced parameter $\tan \beta$ has no *a priori* connection to the Yukawa interaction.

The decompositions for $\Phi_1$ and $\tilde{\Phi}_1 = -i\left[\Phi_1^\dagger \sigma_2\right]^{\mathrm{T}} = i\sigma_2 \Phi_1^*$ are given by

$$\Phi_1 = \begin{pmatrix} \varphi_1^+ \\ \frac{1}{\sqrt{2}}(v_1 + \eta_1 + i\chi_1) \end{pmatrix}, \quad \tilde{\Phi}_1 = \begin{pmatrix} \frac{1}{\sqrt{2}}(v_1 + \eta_1 - i\chi_1) \\ -\varphi_1^- \end{pmatrix} \tag{A.3}$$

and similarly for $\Phi_2$ and $\tilde{\Phi}_2$.

The massless charged Goldstone boson, $G^+$, and the charged Higgs boson, $H^+$, are given as

$$\begin{aligned} G^+ &= \cos \beta \, \varphi_1^+ + \sin \beta \, \varphi_2^+, \\ H^+ &= -\sin \beta \, \varphi_1^+ + \cos \beta \, \varphi_2^+. \end{aligned} \tag{A.4}$$

Inverting these relations, we find

$$\begin{aligned} \varphi_1^+ &= \cos \beta \, G^+ - \sin \beta \, H^+, \\ \varphi_2^+ &= \sin \beta \, G^+ + \cos \beta \, H^+. \end{aligned} \tag{A.5}$$

## Appendix B: Yukawa couplings for the 2HDM

For completeness, we summarize in this appendix the definition of Yukawa couplings in the general 2HDM employed for the analysis in this paper. Below, we also give a comparison with other notations.

### B.1 Our notation

Assuming the SM fermion content (without right-handed neutrinos), couplings of the fermions to two scalar doublets ($a = 1, 2$) may be written in a completely general setting as

$$-\mathcal{L}_{\text{Yukawa}} = \overline{Q}_L \Phi_a F_a^D D_R + \overline{Q}_L \tilde{\Phi}_a F_a^U U_R + \overline{L}_L \Phi_a F_a^L L_R + \text{h.c.}, \tag{B.1}$$

**Table 6** Relevant vacuum expectation values, for $\Phi_1$ or $\Phi_2$, denoted 1 and 2, and reduced Yukawa couplings $\mathcal{F}$, as defined by Eq. (B.2) for models without tree-level FCNC

| Fermion | $D$ | | $U$ | | $L$ | |
|---|---|---|---|---|---|---|
| Model | vev | $\mathcal{F}^D$ | vev | $\mathcal{F}^U$ | vev | $\mathcal{F}^L$ |
| I | 2 | $-\cot\beta$ | 2 | $+\cot\beta$ | 2 | $-\cot\beta$ |
| II | 1 | $+\tan\beta$ | 2 | $+\cot\beta$ | 1 | $+\tan\beta$ |
| X | 2 | $-\cot\beta$ | 2 | $+\cot\beta$ | 1 | $+\tan\beta$ |
| Y | 1 | $+\tan\beta$ | 2 | $+\cot\beta$ | 2 | $-\cot\beta$ |

**Table 7** Dictionary of notations. "HHG": Higgs Hunter's Guide [6]. "BHP": Barger, Hewett, Phillips [296]. "G": Grossman [191], "AS": Akeroyd, Stirling [15]. The (*) denotes interchange $\Phi_1 \leftrightarrow \Phi_2$. "ARS": Atwood, Reina, Soni [297]. "AKTY": Aoki, Kanemura, Tsumura, Yagyu [298]. "BFLRSS": Branco, Ferreira, Lavoura, Rebelo, Sher, Silva [7]

| $\Phi_1$ | $\Phi_2$ | This work | HHG | BHP | G, AS | ARS | AKTY | BFLRSS |
|---|---|---|---|---|---|---|---|---|
| | $u, d, \ell$ | I | I | I | I (*) | – | I | I |
| $d, \ell$ | $u$ | II | II | II | II | – | II | II |
| $u, d, \ell$ | $u, d, \ell$ | III | – | – | – | III | – | III |
| $\ell$ | $u, d$ | X | – | IV | I' (*) | – | X | Lepton specific |
| $d$ | $u, \ell$ | Y | – | III | II' | – | Y | Flipped |

where $\tilde{\Phi}_a$ are defined above as charge conjugate doublets with hypercharge opposite to $\Phi_a$.

The Lagrangian is written in the basis of weak eigenstates, i.e. $Q_L$ and $L_L$ are SU(2) doublets, while $U_R$, $D_R$, and $L_R$ are singlets. The fermions are 3-component vectors in flavor space. Consequently, the Yukawa couplings $F_a^F$ are $3 \times 3$ complex matrices.

There are various ways fermions can couple to the Higgs doublets, leading to different Yukawa couplings. Since an extended Higgs sector naturally leads to FCNC, these would have to be suppressed. This is normally achieved by imposing discrete symmetries in modeling the Yukawa interactions, as for example $Z_2$ symmetry under the transformation $\Phi_1 \to \Phi_1, \Phi_2 \to -\Phi_2$. There are four such possible models with Natural Flavor Conservation (NFC): all fermions couple only to *one* doublet (conventionally taken to be $\Phi_2$), or one fermion $(U, D, L)$ couples to one doublet, the other two to the other doublet.[20] Still other Yukawa models are being considered, where all fermions couple to both doublets (Model III), leading to tree-level FCNC processes. This issue is discussed in Appendix B.3 below.

In the three-generation case with discrete symmetry imposed on the Yukawa Lagrangian, such that each right-handed fermionic state interacts with only one scalar doublet, we have for the fermion mass eigenstates

$$\mathcal{L}_{\text{ch}} = \frac{g}{\sqrt{2}m_W} \left\{ \left[ V_{\text{CKM}} \overline{U} \left( M_D^{\text{diag}} P_R \mathcal{F}^D + M_U^{\text{diag}} P_L \mathcal{F}^U \right) D \right. \right.$$
$$\left. \left. + \overline{N} M_L^{\text{diag}} P_R \mathcal{F}^L L \right] H^+ + \text{h.c.} \right\}, \quad \text{(B.2)}$$

where we used a notation like in Eq. (B.1), with $N$ referring to the neutrinos. Here, $P_L$ and $P_R$ are chirality projection operators. The couplings $\mathcal{F}^D$, $\mathcal{F}^U$ defining models of Yukawa interactions are given in Table 6 for the notation that is used in this paper. Note the appearance of the $V_{CKM}$ matrix.

---

[20] Avoiding FCNC at tree level may not be sufficient, however. One should also investigate stability of these conditions under radiative corrections [295].

We can write the charged-Higgs Lagrangian for one generation in the simplified form (neglecting elements of the CKM matrix)

$$\mathcal{L}_{\text{ch}} = \frac{g}{\sqrt{2}m_W} \left\{ \left[ \overline{u}(m_d P_R \mathcal{F}^D + m_u P_L \mathcal{F}^U) D \right. \right.$$
$$\left. \left. + \overline{v} m_\ell P_R \mathcal{F}^L \ell \right] H^+ + \text{h.c.} \right\}. \quad \text{(B.3)}$$

For Model II we have

$$\mathcal{L}_{\text{ch}}^{II} = \frac{g}{\sqrt{2}m_W} \overline{u} \left[ m_d P_R \tan\beta + m_u P_L \cot\beta \right] d H^+ + \text{h.c.} \quad \text{(B.4)}$$

(see Eq. (4.2)).

For Model I we have

$$\mathcal{L}_{\text{ch}}^{I} = \frac{g \cot\beta}{\sqrt{2}m_W} \overline{u} \left[ -m_d P_R + m_u P_L \right] d H^+ + \text{h.c.} \quad \text{(B.5)}$$

In the limit that in the above equation the second term dominates (for example, for the third generation, with $m_t \gg m_b$) these couplings are the same as for Model II, for moderate values of $\tan\beta$.

### B.2 Various notations

The 1981 paper by Hall and Wise [299] may have been the first to introduce "Model I" and "Model II". They were introduced in analogy with the later convention of "The Higgs Hunter's Guide" (see below), but with the role of $\Phi_1$ and $\Phi_2$ interchanged. An early paper distinguishing quarks and leptons in this respect, was that of Barnett, Senjanovic, Wolfenstein, and Wyler [300]. They define models IA, IB, IIA, IIB.

The definitions of "Model I" and "Model II" presented above coincide with those of the "Higgs Hunter's Guide" [6]. Barger, Hewett and Phillips [296] defined additional models, where quarks and leptons couple differently. Also Grossman [191], Akeroyd and Stirling [15] discussed such models, under different names. Aoki, Kanemura, Tsumura, and Yagyu [298] introduced "Model X" and "Model Y" to

avoid the ambiguity previously associated with "Model III". We have adopted the latter notation in this paper.

In Table 7 we present a "dictionary" of notations for the five models.

### B.3 Minimal flavor violation

In the most general version of the 2HDM, the fermionic couplings of the neutral scalars are non-diagonal in flavor, leading to FCNC at the tree level.

In Refs. [301,302], the authors propose the so-called *aligned* 2HDM by fixing the matrices $F_a^F$ in Eq. (B.1), for $a = 1$ and $a = 2$, to be pairwise proportional,

$$F_1^D \sim F_2^D \sim Y^D, \quad F_1^U \sim F_2^U \sim Y^U. \tag{B.6}$$

Thus, there is no FCNC at tree level.

The aligned 2HDM is just the most general minimally flavor-violating (MFV) renormalizable 2HDM, with the lowest order in the couplings $Y^F$.

Following Ref. [303], the most general MFV ansatz is given by the expansion

$$
\begin{aligned}
F_1^D &= Y^D, \\
F_2^D &= \epsilon_0 Y^D + \epsilon_1 Y^D (Y^D)^\dagger Y^D + \epsilon_2 Y^U (Y^U)^\dagger Y^D + \cdots, \\
F_1^U &= \epsilon'_0 Y^U + \epsilon'_1 Y^U (Y^U)^\dagger Y^U + \epsilon'_2 Y^D (Y^D)^\dagger Y^U + \cdots, \\
F_2^U &= Y^U.
\end{aligned}
\tag{B.7}
$$

This simple form of $F_1^D$ and $F_2^U$ can be assumed without loss of generality. But even if the higher-order terms in $F_2^D$ and $F_1^U$ are not included at tree level, they are generated by radiative corrections. This is ensured by the RG invariance of the MFV hypothesis which is implemented by the *flavor* $SU(3)^3$ symmetry. Thus, the functional form of Eq. (B.7) is preserved, only the coefficients $\epsilon_i$ and $\epsilon'_i$ change and become related via the RG equations. In view of this, it is also clear that setting all $\epsilon$ coefficients to zero leads to heavy fine-tuning. Thus, in general there is no Yukawa alignment within the MFV framework.

In Ref. [295], the stability of the various tree-level implementations is discussed. In the MFV case, the FCNC induced by higher-order terms are under control, since even when the coefficients in Eq. (B.7) are of $\mathcal{O}(1)$ the expansion is rapidly convergent due to small CKM matrix elements and small quark masses [303].

The higher-dimensional operators which are $Z_2$ invariant may still induce new FCNC and further flavor protection is needed [295], e.g. via the MFV hypothesis. This problem already occurs in the case of one Higgs doublet [304–306].

### References

1. ATLAS, G. Aad et al. Phys. Lett. B **716**, 1 (2012). arXiv:1207.7214
2. CMS, S. Chatrchyan et al. Phys. Lett. B **716**, 30 (2012). arXiv:1207.7235
3. CMS, V. Khachatryan et al., Eur. Phys. J. C **75**, 212 (2015). arXiv:1412.8662
4. ATLAS, G. Aad et al., JHEP **08**, 137 (2015). arXiv:1506.06641
5. ATLAS, CMS, G. Aad et al., Phys. Rev. Lett. **114**, 191803 (2015). arXiv:1503.07589
6. J.F. Gunion, H.E. Haber, G.L. Kane, S. Dawson, *The Higgs Hunter's Guide* (Addison-Wesley Publishing Company, Boston, 1990)
7. G. Branco et al., Phys. Rept. **516**, 1 (2012). arXiv:1106.0034
8. D.A. Ross, M.J.G. Veltman, Nucl. Phys. B **95**, 135 (1975)
9. M.J.G. Veltman, Acta Phys. Polon. B **8**, 475 (1977)
10. M.J.G. Veltman, Nucl. Phys. B **123**, 89 (1977)
11. S.L. Glashow, S. Weinberg, Phys. Rev. D **15**, 1958 (1977)
12. F.E. Paige, E.A. Paschos, T. Trueman, Phys. Rev. D **15**, 3416 (1977)
13. M. Misiak et al., Phys. Rev. Lett. **114**, 221801 (2015). arXiv:1503.01789
14. M. Misiak, M. Steinhauser, Eur. Phys. J. C **77**, 201 (2017). arXiv:1702.04571
15. A. Akeroyd, W. Stirling, Nucl. Phys. B **447**, 3 (1995)
16. H.E. Logan, D. MacLennan, Phys. Rev. D **79**, 115022 (2009). arXiv:0903.2246
17. ALEPH, DELPHI, L3, OPAL, LEP, G. Abbiendi et al., Eur. Phys. J. C **73**, 2463 (2013). arXiv:1301.6065
18. T.D. Lee, Phys. Rev. D **8**, 1226 (1973)
19. A. Riotto, M. Trodden, Ann. Rev. Nucl. Part. Sci. **49**, 35 (1999). arXiv:hep-ph/9901362
20. E. Accomando et al., Report of the Workshop on CP Studies and Non-standard Higgs Physics, CERN, Geneva, Switzerland, May 2004–Dec 2005 (2006). arXiv:hep-ph/0608079
21. A.W. El Kaffas, P. Osland, O.M. Ogreid, Nonlinear. Phenom. Complex Syst. **10**, 347 (2007). arXiv:hep-ph/0702097
22. A.W. El Kaffas, W. Khater, O.M. Ogreid, P. Osland, Nucl. Phys. B **775**, 45 (2007). arXiv:hep-ph/0605142
23. I.F. Ginzburg, JETP Lett. **99**, 742 (2014). arXiv:1410.0873
24. S. Nie, M. Sher, Phys. Lett. B **449**, 89 (1999). arXiv:hep-ph/9811234
25. P. Ferreira, R. Santos, A. Barroso, Phys. Lett. B **603**, 219 (2004). arXiv:hep-ph/0406231
26. A. Goudelis, B. Herrmann, O. Stål, JHEP **1309**, 106 (2013). arXiv:1303.3010
27. B. Swiezewska, JHEP **07**, 118 (2015). arXiv:1503.07078
28. N. Khan, S. Rakshit, Phys. Rev. D **92**, 055006 (2015). arXiv:1503.03085
29. N.G. Deshpande, E. Ma, Phys. Rev. D **18**, 2574 (1978)
30. S. Kanemura, T. Kasai, Y. Okada, Phys. Lett. B **471**, 182 (1999). arXiv:hep-ph/9903289
31. A. Barroso, P. Ferreira, I. Ivanov, R. Santos, JHEP **1306**, 045 (2013). arXiv:1303.5098
32. I. Ginzburg, K. Kanishev, M. Krawczyk, D. Sokolowska, Phys. Rev. D **82**, 123533 (2010). arXiv:1009.4593
33. B. Swiezewska, Phys. Rev. D **88**, 055027 (2013). arXiv:1209.5725
34. S. Kanemura, T. Kubota, E. Takasugi, Phys. Lett. B **313**, 155 (1993). arXiv:hep-ph/9303263
35. A.G. Akeroyd, A. Arhrib, E.-M. Naimi, Phys. Lett. B **490**, 119 (2000). arXiv:hep-ph/0006035
36. A. Arhrib, (2000). arXiv:hep-ph/0012353, based on hep-ph/0006035

37. I. Ginzburg, I. Ivanov (2003). arXiv:hep-ph/0312374
38. I. Ginzburg, I. Ivanov, Phys. Rev. D **72**, 115010 (2005). arXiv:hep-ph/0508020
39. A. Wahab El Kaffas, P. Osland, O.M. Ogreid, Phys. Rev. D **76**, 095001 (2007). arXiv:0706.2997
40. B. Gorczyca, M. Krawczyk, (2011). arXiv:1112.5086
41. B. Grinstein, C.W. Murphy, P. Uttayarat, JHEP **06**, 070 (2016). arXiv:1512.04567
42. D.C. Kennedy, B.W. Lynn, Nucl. Phys. B **322**, 1 (1989)
43. M.E. Peskin, T. Takeuchi, Phys. Rev. Lett. **65**, 964 (1990)
44. G. Altarelli, R. Barbieri, Phys. Lett. B **253**, 161 (1991)
45. M.E. Peskin, T. Takeuchi, Phys. Rev. D **46**, 381 (1992)
46. G. Altarelli, R. Barbieri, S. Jadach, Nucl. Phys. B **369**, 3 (1992). [Erratum: Nucl. Phys. B **376**, 444 (1992)]
47. W. Grimus, L. Lavoura, O. Ogreid, P. Osland, J. Phys. G **35**, 075001 (2008). arXiv:0711.4022
48. W. Grimus, L. Lavoura, O. Ogreid, P. Osland, Nucl. Phys. B **801**, 81 (2008). arXiv:0802.4353
49. M. Jung, A. Pich, P. Tuzon, JHEP **1011**, 003 (2010). arXiv:1006.0470
50. J.F. Gunion, H.E. Haber, Nucl. Phys. B **278**, 449 (1986). [Erratum: Nucl. Phys. B **402**, 569 (1993)]
51. S. Moretti, W. Stirling, Phys. Lett. B **347**, 291 (1995). arXiv:hep-ph/9412209
52. A. Djouadi, J. Kalinowski, P. Zerwas, Z. Phys. C **70**, 435 (1996). arXiv:hep-ph/9511342
53. A. Djouadi, J. Kalinowski, M. Spira, Comput. Phys. Commun. **108**, 56 (1998). arXiv:hep-ph/9704448
54. S. Kanemura, S. Moretti, Y. Mukai, R. Santos, K. Yagyu, Phys. Rev. D **79**, 055017 (2009). arXiv:0901.0204
55. D. Eriksson, J. Rathsman, O. Stål, Comput. Phys. Commun. **181**, 189 (2010). arXiv:0902.0851
56. R. Harlander, M.Mühlleitner, J. Rathsman, M. Spira, O. Stål, (2013). arXiv:1312.5571
57. A. Mendez, A. Pomarol, Phys. Lett. B **252**, 461 (1990)
58. C.-S. Li, R.J. Oakes, Phys. Rev. D **43**, 855 (1991)
59. A. Djouadi, P. Gambino, Phys. Rev. D **51**, 218 (1995). arXiv:hep-ph/9406431, [Erratum: Phys. Rev. D **53**, 4111 (1996)]
60. D. Fontes, J.C. Romão, R. Santos, J.P. Silva, Phys. Rev. D **92**, 055014 (2015). arXiv:1506.06755
61. V. Keus, S.F. King, S. Moretti, K. Yagyu, JHEP **04**, 048 (2016). arXiv:1510.04028
62. L. Basso, P. Osland, G.M. Pruna, JHEP **06**, 083 (2015). arXiv:1504.07552
63. D. Dicus, J. Hewett, C. Kao, T. Rizzo, Phys. Rev. D **40**, 787 (1989)
64. A.A.B. Bendezu, B.A. Kniehl, Phys. Rev. D **59**, 015009 (1999). arXiv:hep-ph/9807480
65. S. Moretti, K. Odagiri, Phys. Rev. D **59**, 055008 (1999). arXiv:hep-ph/9809244
66. A.B. Bendezu, B.A. Kniehl., Phys. Rev. D **61**, 097701 (2000). arXiv:hep-ph/9909502
67. O. Brein, W. Hollik, S. Kanemura, Phys. Rev. D **63**, 095001 (2001). arXiv:hep-ph/0008308
68. W. Hollik, S.-H. Zhu, Phys. Rev. D **65**, 075015 (2002). arXiv:hep-ph/0109103
69. E. Asakawa, O. Brein, S. Kanemura, Phys. Rev. D **72**, 055017 (2005). arXiv:hep-ph/0506249
70. D. Eriksson, S. Hesselbach, J. Rathsman, Eur. Phys. J. C **53**, 267 (2008). arXiv:hep-ph/0612198
71. M. Hashemi, Phys. Rev. D **83**, 055004 (2011). arXiv:1008.3785
72. J. Gunion, H. Haber, F. Paige, W.-K. Tung, S. Willenbrock, Nucl. Phys. B **294**, 621 (1987)
73. J. Diaz-Cruz, O. Sampayo, Phys. Rev. D **50**, 6820 (1994)
74. S. Moretti, K. Odagiri, Phys. Rev. D **55**, 5627 (1997). arXiv:hep-ph/9611374
75. D. Miller, S. Moretti, D. Roy, W. Stirling, Phys. Rev. D **61**, 055011 (2000). arXiv:hep-ph/9906230
76. S. Moretti, D. Roy, Phys. Lett. B **470**, 209 (1999). arXiv:hep-ph/9909435
77. S.-H. Zhu, Phys. Rev. D **67**, 075006 (2003). arXiv:hep-ph/0112109
78. T. Plehn, Phys. Rev. D **67**, 014018 (2003). arXiv:hep-ph/0206121
79. E.L. Berger, T. Han, J. Jiang, T. Plehn, Phys. Rev. D **71**, 115012 (2005). arXiv:hep-ph/0312286
80. N. Kidonakis, JHEP **05**, 011 (2005). arXiv:hep-ph/0412422
81. C. Weydert et al., Eur. Phys. J. C **67**, 617 (2010). arXiv:0912.3430
82. N. Kidonakis, Phys. Rev. D **82**, 054018 (2010). arXiv:1005.4451
83. M. Flechl, R. Klees, M. Kramer, M. Spira, M. Ubiali, Phys. Rev. D **91**, 075015 (2015). arXiv:1409.5615
84. C. Degrande, M. Ubiali, M. Wiesemann, M. Zaro, JHEP **10**, 145 (2015). arXiv:1507.02549
85. N. Kidonakis, Phys. Rev. D **94**, 014010 (2016). arXiv:1605.00622
86. C. Degrande et al. (2016). arXiv:1607.05291
87. F. Borzumati, J.-L. Kneur, N. Polonsky, Phys. Rev. D **60**, 115011 (1999). arXiv:hep-ph/9905443
88. J. Alwall, J. Rathsman, JHEP **0412**, 050 (2004). arXiv:hep-ph/0409094
89. H.-J. He, C. Yuan, Phys. Rev. Lett. **83**, 28 (1999). arXiv:hep-ph/9810367
90. J. Diaz-Cruz, H.-J. He, C. Yuan, Phys. Lett. B **530**, 179 (2002). arXiv:hep-ph/0103178
91. S. Slabospitsky, (2002). arXiv:hep-ph/0203094
92. S. Dittmaier, G. Hiller, T. Plehn, M. Spannowsky, Phys. Rev. D **77**, 115001 (2008). arXiv:0708.0940
93. R. Harlander, M. Kramer, M. Schumacher, (2011). arXiv:1112.3478
94. R.M. Barnett, H.E. Haber, D.E. Soper, Nucl. Phys. B **306**, 697 (1988)
95. F.I. Olness, W.-K. Tung, Nucl. Phys. B **308**, 813 (1988)
96. LHC Higgs Cross Section Working Group, D. de Florian et al., (2016). arXiv:1610.07922
97. A. Belyaev, D. Garcia, J. Guasch, J. Sola, Phys. Rev. D **65**, 031701 (2002). arXiv:hep-ph/0105053
98. A. Belyaev, D. Garcia, J. Guasch, J. Sola, JHEP **06**, 059 (2002). arXiv:hep-ph/0203031
99. M. Guchait, S. Moretti, JHEP **0201**, 001 (2002). arXiv:hep-ph/0110020
100. J. Alwall, C. Biscarat, S. Moretti, J. Rathsman, A. Sopczak, Eur. Phys. J. C **39S1**, 37 (2005). arXiv:hep-ph/0312301
101. K. Assamagan, M. Guchait, S. Moretti (2004). arXiv:hep-ph/0402057
102. S. Kanemura, C. Yuan, Phys. Lett. B **530**, 188 (2002). arXiv:hep-ph/0112165
103. A.G. Akeroyd, M.A. Diaz, Phys. Rev. D **67**, 095007 (2003). arXiv:hep-ph/0301203
104. A. Akeroyd, Phys. Rev. D **68**, 077701 (2003). arXiv:hep-ph/0306045
105. Q.-H. Cao, S. Kanemura, C. Yuan, Phys. Rev. D **69**, 075008 (2004). arXiv:hep-ph/0311083
106. A. Belyaev, Q.-H. Cao, D. Nomura, K. Tobe, C.-P. Yuan, Phys. Rev. Lett. **100**, 061801 (2008). arXiv:hep-ph/0609079
107. X. Miao, S. Su, B. Thomas, Phys. Rev. D **82**, 035009 (2010). arXiv:1005.0090
108. E. Eichten, I. Hinchliffe, K.D. Lane, C. Quigg, Rev. Mod. Phys. **56**, 579 (1984)
109. S.S. Willenbrock, Phys. Rev. D **35**, 173 (1987)
110. E. Glover, J. van der Bij, Nucl. Phys. B **309**, 282 (1988)
111. D.A. Dicus, C. Kao, S.S. Willenbrock, Phys. Lett. B **203**, 457 (1988)
112. Y. Jiang, L. Han, W.-G. Ma, Z.-H. Yu, M. Han, J. Phys. G **23**, 385 (1997). arXiv:hep-ph/9703275

113. A. Krause, T. Plehn, M. Spira, P. Zerwas, Nucl. Phys. B **519**, 85 (1998). arXiv:hep-ph/9707430
114. A.B. Bendezu, B.A. Kniehl., Nucl. Phys. B **568**, 305 (2000). arXiv:hep-ph/9908385
115. O. Brein, W. Hollik, Eur. Phys. J. C **13**, 175 (2000). arXiv:hep-ph/9908529
116. S. Moretti, J. Phys. G **28**, 2567 (2002). arXiv:hep-ph/0102116
117. S. Moretti, J. Rathsman, Eur. Phys. J. C **33**, 41 (2004). arXiv:hep-ph/0308215
118. A. Alves, T. Plehn, Phys. Rev. D **71**, 115014 (2005). arXiv:hep-ph/0503135
119. J. Pumplin et al., JHEP **0207**, 012 (2002). arXiv:hep-ph/0201195
120. M. Spira, A. Djouadi, D. Graudenz, P.M. Zerwas, Nucl. Phys. B **453**, 17 (1995). arXiv:hep-ph/9504378
121. L. Basso et al., JHEP **1211**, 011 (2012). arXiv:1205.6569
122. L. Basso et al., PoS Corf. **2012**, 029 (2013). arXiv:1305.3219
123. M. Beneke, P. Falgari, S. Klein, C. Schwinn, Nucl. Phys. B **855**, 695 (2012). arXiv:1109.1536
124. M. Cacciari, M. Czakon, M. Mangano, A. Mitov, P. Nason, Phys. Lett. B **710**, 612 (2012). arXiv:1111.5869
125. M. Czakon, A. Mitov, Comput. Phys. Commun. **185**, 2930 (2014). arXiv:1112.5675
126. P. Bärnreuther, M. Czakon, A. Mitov, Phys. Rev. Lett. **109**, 132001 (2012). arXiv:1204.5201
127. M. Czakon, A. Mitov, JHEP **12**, 054 (2012). arXiv:1207.0236
128. M. Czakon, A. Mitov, JHEP **01**, 080 (2013). arXiv:1210.6832
129. M. Czakon, P. Fiedler, A. Mitov, Phys. Rev. Lett. **110**, 252004 (2013). arXiv:1303.6254
130. A. Czarnecki, K. Melnikov, Nucl. Phys. B **544**, 520 (1999). arXiv:hep-ph/9806244
131. K.G. Chetyrkin, R. Harlander, T. Seidensticker, M. Steinhauser, Phys. Rev. D **60**, 114015 (1999). arXiv:hep-ph/9906273
132. I.R. Blokland, A. Czarnecki, M. Slusarczyk, F. Tkachov, Phys. Rev. Lett. **93**, 062001 (2004). arXiv:hep-ph/0403221
133. I.R. Blokland, A. Czarnecki, M. Slusarczyk, F. Tkachov, Phys. Rev. D **71**, 054004 (2005). arXiv:hep-ph/0503039, [Erratum: Phys. Rev. D **79**, 019901 (2009)]
134. A. Czarnecki, J.G. Korner, J.H. Piclum, Phys. Rev. D **81**, 111503 (2010). arXiv:1005.2625
135. J. Gao, C.S. Li, H.X. Zhu, Phys. Rev. Lett. **110**, 042001 (2013). arXiv:1210.2808
136. M. Brucherseifer, F. Caola, K. Melnikov, JHEP **04**, 059 (2013). arXiv:1301.7133
137. A. Czarnecki, S. Davidson, Phys. Rev. D **48**, 4183 (1993). arXiv:hep-ph/9301237
138. F. Mahmoudi, O. Stal, Phys. Rev. D **81**, 035016 (2010). arXiv:0907.1791
139. A. Crivellin, A. Kokulu, C. Greub, Phys. Rev. D **87**, 094031 (2013). arXiv:1303.5877
140. P. Krawczyk, S. Pokorski, Phys. Rev. Lett. **60**, 182 (1988)
141. J.M. Cline, Phys. Rev. D **93**, 075017 (2016). arXiv:1512.02210
142. A. Crivellin, J. Heeck, P. Stoffer, Phys. Rev. Lett. **116**, 081801 (2016). arXiv:1507.07567
143. O.P.A.L. Collaboration, G. Abbiendi et al., Phys. Lett. B **520**, 1 (2001). arXiv:hep-ex/0108031
144. M. Krawczyk, D. Temes, Eur. Phys. J. C **44**, 435 (2005). arXiv:hep-ph/0410248
145. Particle Data Group, K.A. Olive et al., Chin. Phys. C **38**, 090001 (2014)
146. Heavy Flavor Averaging Group (HFAG), Y. Amhis et al., (2014). arXiv:1412.7515
147. CKMfitter Group, J. Charles et al., Eur. Phys. J. C **41**, 1 (2005). arXiv:hep-ph/0406184
148. W.-S. Hou, Phys. Rev. D **48**, 2342 (1993)
149. Y. Grossman, Z. Ligeti, Phys. Lett. B **332**, 373 (1994). arXiv:hep-ph/9403376
150. Y. Grossman, H.E. Haber, Y. Nir, Phys. Lett. B **357**, 630 (1995). arXiv:hep-ph/9507213
151. BABAR Collaboration, B. Aubert et al., Phys. Rev. Lett. **100**, 021801 (2008). arXiv:0709.1698
152. U. Nierste, S. Trine, S. Westhoff, Phys. Rev. D **78**, 015006 (2008). arXiv:0801.4938
153. BABAR, J.P. Lees et al. Phys. Rev. Lett. **109**, 101802 (2012). arXiv:1205.5442
154. BABAR, J. Lees et al., Phys. Rev. D **88**, 072012 (2013). arXiv:1303.0571
155. Belle, M. Huschle et al., Phys. Rev. D **92**, 072014 (2015). arXiv:1507.03233
156. Belle, A. Abdesselam et al., (2016). arXiv:1603.06711
157. LHCb, R. Aaij et al., Phys. Rev. Lett. **115**, 111803 (2015). arXiv:1506.08614, [Addendum: Phys. Rev. Lett. **115**, no. 15, 159901(2015)]
158. M. Freytsis, Z. Ligeti, J.T. Ruderman, Phys. Rev. D **92**, 054018 (2015). arXiv:1506.08896
159. S. Fajfer, J.F. Kamenik, I. Nisandzic, Phys. Rev. D **85**, 094025 (2012). arXiv:1203.2654
160. MILCs, J.A. Bailey et al., Phys. Rev. D **92**, 034506 (2015). arXiv:1503.07237
161. HPQCD, H. Na, C.M. Bouchard, G.P. Lepage, C. Monahan, J. Shigemitsu, Phys. Rev. D **92**, 054510 (2015). arXiv:1505.03925
162. A. Akeroyd, F. Mahmoudi, JHEP **0904**, 121 (2009). arXiv:0902.2393
163. T. Hermann, M. Misiak, M. Steinhauser, JHEP **11**, 036 (2012). arXiv:1208.2788
164. K.G. Chetyrkin, M. Misiak, M. Munz, Phys. Lett. B **400**, 206 (1997). arXiv:hep-ph/9612313
165. A.J. Buras, A. Kwiatkowski, N. Pott, Phys. Lett. B **414**, 157 (1997). arXiv:hep-ph/9707482
166. C.W. Bauer, Phys. Rev. D **57**, 5611 (1998). arXiv:hep-ph/9710513
167. C. Bobeth, M. Misiak, J. Urban, Nucl. Phys. B **574**, 291 (2000). arXiv:hep-ph/9910220
168. A.J. Buras, A. Czarnecki, M. Misiak, J. Urban, Nucl. Phys. B **631**, 219 (2002). arXiv:hep-ph/0203135
169. M. Misiak, M. Steinhauser, Nucl. Phys. B **683**, 277 (2004). arXiv:hep-ph/0401041
170. M. Neubert, Eur. Phys. J. C **40**, 165 (2005). arXiv:hep-ph/0408179
171. K. Melnikov, A. Mitov, Phys. Lett. B **620**, 69 (2005). arXiv:hep-ph/0505097
172. M. Misiak et al., Phys. Rev. Lett. **98**, 022002 (2007). arXiv:hep-ph/0609232
173. M. Misiak, M. Steinhauser, Nucl. Phys. B **764**, 62 (2007). arXiv:hep-ph/0609241
174. H.M. Asatrian, T. Ewerth, H. Gabrielyan, C. Greub, Phys. Lett. B **647**, 173 (2007). arXiv:hep-ph/0611123
175. M. Czakon, U. Haisch, M. Misiak, JHEP **03**, 008 (2007). arXiv:hep-ph/0612329
176. R. Boughezal, M. Czakon, T. Schutzmeier, JHEP **09**, 072 (2007). arXiv:0707.3090
177. T. Ewerth, Phys. Lett. B **669**, 167 (2008). arXiv:0805.3911
178. M. Misiak, M. Steinhauser, Nucl. Phys. B **840**, 271 (2010). arXiv:1005.1173
179. H.M. Asatrian, T. Ewerth, A. Ferroglia, C. Greub, G. Ossola, Phys. Rev. D **82**, 074006 (2010). arXiv:1005.5587
180. A. Ferroglia, U. Haisch, Phys. Rev. D **82**, 094012 (2010). arXiv:1009.2144
181. M. Misiak, M. Poradzinski, Phys. Rev. D **83**, 014024 (2011). arXiv:1009.5685
182. M. Kaminski, M. Misiak, M. Poradzinski, Phys. Rev. D **86**, 094004 (2012). arXiv:1209.0965
183. M. Czakon et al., JHEP **04**, 168 (2015). arXiv:1503.01791
184. P. Ciafaloni, A. Romanino, A. Strumia, Nucl. Phys. B **524**, 361 (1998). arXiv:hep-ph/9710312

185. M. Ciuchini, G. Degrassi, P. Gambino, G.F. Giudice, Nucl. Phys. B **527**, 21 (1998). arXiv:hep-ph/9710335
186. F. Borzumati, C. Greub, Phys. Rev. D **58**, 074004 (1998). arXiv:hep-ph/9802391
187. C. Bobeth, M. Misiak, J. Urban, Nucl. Phys. B **567**, 153 (2000). arXiv:hep-ph/9904413
188. P. Gambino, M. Misiak, Nucl. Phys. B **611**, 338 (2001). arXiv:hep-ph/0104034
189. K. Trabelsi, (2015). Talk given at EPS conference. http://eps-hep2015.eu/
190. Belle, T. Saito et al., Phys. Rev. D **91**, 052004 (2015). arXiv:1411.7198
191. Y. Grossman, Nucl. Phys. B **426**, 355 (1994). arXiv:hep-ph/9401311
192. L. Abbott, P. Sikivie, M.B. Wise, Phys. Rev. D **21**, 1393 (1980)
193. T. Inami, C. Lim, Progr. Theor. Phys. **65**, 297 (1981)
194. G.G. Athanasiu, P.J. Franzini, F.J. Gilman, Phys. Rev. D **32**, 3010 (1985)
195. S.L. Glashow, E.E. Jenkins, Phys. Lett. B **196**, 233 (1987)
196. C. Geng, J.N. Ng, Phys. Rev. D **38**, 2857 (1988)
197. J. Urban, F. Krauss, U. Jentschura, G. Soff, Nucl. Phys. B **523**, 40 (1998). arXiv:hep-ph/9710245
198. O. Deschamps et al., Phys. Rev. D **82**, 073012 (2010). arXiv:0907.5135
199. M. Gorbahn, J.M. No, V. Sanz, JHEP **10**, 036 (2015). arXiv:1502.07352
200. K. Cheung, O.C. Kong, Phys. Rev. D **68**, 053003 (2003). arXiv:hep-ph/0302111
201. D. Chang, W.-F. Chang, C.-H. Chou, W.-Y. Keung, Phys. Rev. D **63**, 091301 (2001). arXiv:hep-ph/0009292
202. M. Krawczyk, Acta Phys. Polon. B **33**, 2621 (2002). arXiv:hep-ph/0208076, Dedicated to Stefan Pokorski on the occasion of his 60th birthday
203. B. Regan, E. Commins, C. Schmidt, D. DeMille, Phys. Rev. Lett. **88**, 071805 (2002)
204. A. Pilaftsis, Nucl. Phys. B **644**, 263 (2002). arXiv:hep-ph/0207277
205. ACME, J. Baron et al., Science **343**, 269 (2014). arXiv:1310.7534
206. S.M. Barr, A. Zee, Phys. Rev. Lett. **65**, 21 (1990)
207. H. Flacher et al., Eur. Phys. J. C **60**, 543 (2009). arXiv:0811.0009, [Erratum: Eur. Phys. J. C **71**, 1718 (2011)]
208. UTfit, M. Bona et al., Phys. Lett. B **687**, 61 (2010). arXiv:0908.3470
209. T. Enomoto, R. Watanabe, JHEP **05**, 002 (2016). arXiv:1511.05066
210. A. Denner, R. Guth, W. Hollik, J.H. Kuhn, Z. Phys. C **51**, 695 (1991)
211. D0 Collaboration, V. Abazov et al., Phys. Lett. B **682**, 278 (2009). arXiv:0908.1811
212. H.E. Logan, D. MacLennan, Phys. Rev. D **81**, 075016 (2010). arXiv:1002.4916
213. C.D.F. Collaboration, T. Aaltonen et al., Phys. Rev. Lett. **103**, 101803 (2009). arXiv:0907.1269
214. D0 Collaboration, V. Abazov et al., Phys. Rev. Lett. **102**, 191802 (2009). arXiv:0807.0859
215. CMS, V. Khachatryan et al., JHEP **12**, 178 (2015). arXiv:1510.04252
216. CMS, V. Khachatryan et al., JHEP **11**, 018 (2015). arXiv:1508.07774
217. ATLAS, G. Aad et al., Eur. Phys. J. C **73**, 2465 (2013). arXiv:1302.3694
218. ATLAS, G. Aad et al., JHEP **03**, 088 (2015). arXiv:1412.6663
219. ATLAS, G. Aad et al., JHEP **03**, 127 (2016). arXiv:1512.03704
220. CMS, S. Chatrchyan et al., JHEP **07**, 143 (2012). arXiv:1205.5736
221. G.C. Dorsch, S.J. Huber, K. Mimasu, J.M. No, (2016). arXiv:1601.04545
222. ATLAS, G. Aad et al., JHEP **11**, 206 (2015). arXiv:1509.00672
223. ATLAS Collaboration, G. Aad et al., Phys. Lett. B **710**, 49 (2012). arXiv:1202.1408
224. CMS, S. Chatrchyan et al., Phys. Lett. B **710**, 26 (2012). arXiv:1202.1488
225. ATLAS, G. Aad et al., Eur. Phys. J. C **76**, 6 (2016). arXiv:1507.04548
226. M. Aoki et al., Phys. Rev. D **84**, 055028 (2011). arXiv:1104.3178
227. A. Arhrib, R. Benbrik, C.-H. Chen, R. Guedes, R. Santos, JHEP **0908**, 035 (2009). arXiv:0906.0387
228. S. Moretti, Phys. Lett. B **481**, 49 (2000). arXiv:hep-ph/0003178
229. D.K. Ghosh, S. Moretti, Eur. Phys. J. C **42**, 341 (2005). arXiv:hep-ph/0412365
230. R. Enberg, W. Klemm, S. Moretti, S. Munir, G. Wouda, Nucl. Phys. B **893**, 420 (2015). arXiv:1412.5814
231. S. Moretti, R. Santos, P. Sharma, Phys. Lett. B **760**, 697 (2016). arXiv:1604.04965
232. P.S. Bhupal Dev, A. Pilaftsis, JHEP **12**, 024 (2014). arXiv:1408.3405, [Erratum: JHEP **11**, 147 (2015)]
233. C.G. Lester, D.J. Summers, Phys. Lett. B **463**, 99 (1999). arXiv:hep-ph/9906349
234. B.C. Allanach et al., Les Houches physics at TeV colliders 2005 beyond the standard model working group: summary report, in Physics at TeV colliders. In: Proceedings, Workshop, Les Houches, France, May 2–20, 2005, 2006. arXiv:hep-ph/0602198
235. R.M. Godbole, S.D. Rindani, R.K. Singh, JHEP **12**, 021 (2006). arXiv:hep-ph/0605100
236. K. Huitu, S. Kumar Rai, K. Rao, S.D. Rindani, P. Sharma, JHEP **04**, 026 (2011). arXiv:1012.0527
237. R.M. Godbole, L. Hartgring, I. Niessen, C.D. White, JHEP **01**, 011 (2012). arXiv:1111.0759
238. S.D. Rindani, R. Santos, P. Sharma, JHEP **11**, 188 (2013). arXiv:1307.1158
239. H.E. Haber, O. Stål, Eur. Phys. J. C **75**, 491 (2015). arXiv:1507.04281
240. F. Kling, J.M. No, S. Su, Submitted to: JHEP **1609**, 093 (2016). arXiv:1604.01406
241. B. Coleppa, F. Kling, S. Su, JHEP **12**, 148 (2014). arXiv:1408.4119
242. F. Kling, A. Pyarelal, S. Su, JHEP **11**, 051 (2015). arXiv:1504.06624
243. A. Arhrib, K. Cheung, J.S. Lee, C.-T. Lu, JHEP **05**, 093 (2016). arXiv:1509.00978
244. G. Cree, H.E. Logan, Phys. Rev. D **84**, 055021 (2011). arXiv:1106.4039
245. M. Trott, M.B. Wise, JHEP **1011**, 157 (2010). arXiv:1009.2813
246. A.G. Akeroyd, S. Moretti, K. Yagyu, E. Yildirim, (2016). arXiv:1605.05881
247. A. Akeroyd, Nucl. Phys. B **544**, 557 (1999). arXiv:hep-ph/9806337
248. A. Akeroyd, S. Moretti, J. Hernandez-Sanchez, Phys. Rev. D **85**, 115002 (2012). arXiv:1203.5769
249. B. Patt, F. Wilczek, (2006). arXiv:hep-ph/0605188
250. A. Pierce, J. Thaler, JHEP **08**, 026 (2007). arXiv:hep-ph/0703056
251. E. Ma, Phys. Rev. D **73**, 077301 (2006). arXiv:hep-ph/0601225
252. R. Barbieri, L.J. Hall, V.S. Rychkov, Phys. Rev. D **74**, 015007 (2006). arXiv:hep-ph/0603188
253. L. Lopez Honorez, E. Nezri, J. F. Oliver, M.H. Tytgat, JCAP **0702**, 028 (2007). arXiv:hep-ph/0612275
254. B. Grzadkowski, O. Ogreid, P. Osland, Phys. Rev. D **80**, 055013 (2009). arXiv:0904.2173
255. B. Grzadkowski, O. Ogreid, P. Osland, A. Pukhov, M. Purmohammadi, JHEP **1106**, 003 (2011). arXiv:1012.4680
256. V. Keus, S.F. King, S. Moretti, D. Sokolowska, JHEP **11**, 016 (2014). arXiv:1407.7859

257. V. Keus, S.F. King, S. Moretti, D. Sokolowska, JHEP **11**, 003 (2015). arXiv:1507.08433

258. C. Bonilla, D. Sokolowska, J.L. Diaz-Cruz, M. Krawczyk, N. Darvishi, J. Phys. G **43**, 065001 (2016). arXiv:1412.8730

259. J. McDonald, Phys. Rev. D **50**, 3637 (1994). arXiv:hep-ph/0702143

260. C. Burgess, M. Pospelov, T. ter Veldhuis, Nucl. Phys. B **619**, 709 (2001). arXiv:hep-ph/0011335

261. V. Barger, P. Langacker, M. McCaskey, M.J. Ramsey-Musolf, G. Shaughnessy, Phys. Rev. D **77**, 035005 (2008). arXiv:0706.4311

262. V. Barger, P. Langacker, M. McCaskey, M. Ramsey-Musolf, G. Shaughnessy, Phys. Rev. D **79**, 015018 (2009). arXiv:0811.0393

263. M. Kadastik, K. Kannike, M. Raidal, Phys. Rev. D **81**, 015002 (2010). arXiv:0903.2475

264. M. Kadastik, K. Kannike, M. Raidal, Phys. Rev. D **80**, 085020 (2009). arXiv:0907.1894

265. H. Fritzsch, P. Minkowski, Ann. Phys. **93**, 193 (1975)

266. L.M. Krauss, F. Wilczek, Phys. Rev. Lett. **62**, 1221 (1989)

267. S.P. Martin, Phys. Rev. D **46**, 2769 (1992). arXiv:hep-ph/9207218

268. M. De Montigny, M. Masip, Phys. Rev. D **49**, 3734 (1994). arXiv:hep-ph/9309312

269. Q.-H. Cao, E. Ma, G. Rajasekaran, Phys. Rev. D **76**, 095011 (2007). arXiv:0708.2939

270. E. Dolle, X. Miao, S. Su, B. Thomas, Phys. Rev. D **81**, 035003 (2010). arXiv:0909.3094

271. K. Huitu, K. Kannike, A. Racioppi, M. Raidal, JHEP **1101**, 010 (2011). arXiv:1005.4409

272. P. Osland, A. Pukhov, G. Pruna, M. Purmohammadi, JHEP **1304**, 040 (2013). arXiv:1302.3713

273. A. Ilnicka, M. Krawczyk, T. Robens, Phys. Rev. D **93**, 055026 (2016). arXiv:1508.01671

274. A. Arhrib, Y.-L.S. Tsai, Q. Yuan, T.-C. Yuan, JCAP **1406**, 030 (2014). arXiv:1310.0358

275. V. Keus, S.F. King, S. Moretti, Phys. Rev. D **90**, 075015 (2014). arXiv:1408.0796

276. S. Moretti, D. Rojas, K. Yagyu, JHEP **08**, 116 (2015). arXiv:1504.06432

277. S. Moretti, K. Yagyu, Phys. Rev. D **91**, 055022 (2015). arXiv:1501.06544

278. P. Minkowski, Phys. Lett. B **67**, 421 (1977)

279. T. Yanagida, Conf. Proc. **C7902131**, 95 (1979)

280. M. Gell-Mann, P. Ramond, R. Slansky, Conf. Proc. C **790927**, 315 (1979). In: Supergravity, P. van Nieuwenhuizen, D.Z. Freedman (eds.), North Holland Publ. Co., (1979)

281. S. Glashow, NATO Adv. Study Inst. Ser. B Phys. **59**, 687 (1980). Preliminary version given at Colloquium in Honor of A. Visconti, Marseille-Luminy Univ. (1979)

282. R.N. Mohapatra, G. Senjanovic, Phys. Rev. Lett. **44**, 912 (1980)

283. M. Fukugita, T. Yanagida, Phys. Lett. B **174**, 45 (1986)

284. S.R. Coleman, E.J. Weinberg, Phys. Rev. D **7**, 1888 (1973)

285. T. Hambye, M.H. Tytgat, Phys. Lett. B **659**, 651 (2008). arXiv:0707.0633

286. M. Kadastik, K. Kannike, A. Racioppi, M. Raidal, Phys. Rev. Lett. **104**, 201301 (2010). arXiv:0912.2729

287. M. Kadastik, K. Kannike, A. Racioppi, M. Raidal, JHEP **1205**, 061 (2012). arXiv:1112.3647

288. M. Kadastik, K. Kannike, A. Racioppi, M. Raidal, Phys. Lett. B **694**, 242 (2010). arXiv:0912.3797

289. M. Gustafsson, S. Rydbeck, L. Lopez-Honorez, E. Lundstrom, Phys. Rev. D **86**, 075019 (2012). arXiv:1206.6316

290. G. Belanger et al., Phys. Rev. D **91**, 115011 (2015). arXiv:1503.07367

291. P. Poulose, S. Sahoo, K. Sridhar, Phys. Lett. B **765**, 300 (2017). arXiv:1604.03045

292. K. Cheung, D.K. Ghosh, JHEP **11**, 048 (2002). arXiv:hep-ph/0208254

293. ATLAS, G. Aad et al., Phys. Rev. Lett. **114**, 231801 (2015). arXiv:1503.04233

294. H. Georgi, M. Machacek, Nucl. Phys. B **262**, 463 (1985)

295. A.J. Buras, M.V. Carlucci, S. Gori, G. Isidori, JHEP **1010**, 009 (2010). arXiv:1005.5310

296. V.D. Barger, J. Hewett, R. Phillips, Phys. Rev. D **41**, 3421 (1990)

297. D. Atwood, L. Reina, A. Soni, Phys. Rev. D **55**, 3156 (1997). arXiv:hep-ph/9609279

298. M. Aoki, S. Kanemura, K. Tsumura, K. Yagyu, Phys. Rev. D **80**, 015017 (2009). arXiv:0902.4665

299. L.J. Hall, M.B. Wise, Nucl. Phys. B **187**, 397 (1981)

300. R. Barnett, G. Senjanovic, L. Wolfenstein, D. Wyler, Phys. Lett. B **136**, 191 (1984)

301. A. Pich, P. Tuzon, Phys. Rev. D **80**, 091702 (2009). arXiv:0908.1554

302. P. Tuzon, A. Pich, Acta Phys. Polon. Supp. **3**, 215 (2010). arXiv:1001.0293

303. G. D'Ambrosio, G. Giudice, G. Isidori, A. Strumia, Nucl. Phys. B **645**, 155 (2002). arXiv:hep-ph/0207036

304. G.F. Giudice, O. Lebedev, Phys. Lett. B **665**, 79 (2008). arXiv:0804.1753

305. K. Agashe, R. Contino, Phys. Rev. D **80**, 075016 (2009). arXiv:0906.1542

306. A. Azatov, M. Toharia, L. Zhu, Phys. Rev. D **80**, 035016 (2009). arXiv:0906.1990